JOHANNES KEPLER
UNIVERSITY LINZ

Submitted by
Simon Straßgschwandtner, BSc

Submitted at
Institute of Biophysics

Thesis Supervisor
Univ-Prof. Dr. **Peter Pohl**

July 2022

Nanodisc-assisted Receptor Channel Reconstitution into Giant Unilamellar Vesicles

Master Thesis

to obtain the academic degree of

Diplom-Ingenieur

in the Master's Program

Biophysik

JOHANNES KEPLER UNIVERSITY LINZ
Altenbergerstraße 69
4040 Linz, Austria
www.jku.at
DVR 0093696

Abstract

The isolation of membrane proteins is still major challenge. Most of the time detergent molecules are used to purify and reconstitute membrane proteins. This method is prone to unfolding or missfolding of the protein and labour intensive. In this work a detergent free method to reconstitute proteins is introduced. Glyco-DIBMA is a amphiphilic polymer which is able to dissolve liposomes as well as cell membranes into so called nanodiscs. These are disc shaped particles, where the hydrophobic core of the lipid is shielded by Glyco-DIBMA from the aqueous surrounding. The formation of nanodiscs from liposomes and membrane fractions containing the protein *Gloeobacter* Ligand-gated Ion Channel is verified via fluorescence correlation spectroscopy. The insertion of nanodiscs with and without protein into giant unilamellar vesicles is checked via a single molecule fluorescence microscope.

Contents

1 Introduction

About 20 % to 30 % of all open reading frames are predicted to encode membrane proteins [1]. They play crucial roles in basic cell functions including signal transduction, energy production, nutrient uptake, and cell—cell communication [2]. More than 50 % of the currently marketed drugs treat diseases by targeting membrane proteins [2, 3]. Nevertheless, the isolation of membrane proteins from cells remains a major challenge [4, 5]. Different methods to achieve this goal exists, some of them will be introduced in the following sections.

1.1 Detergents

Often detergents are used to extract and reconstitute membrane proteins into artificial systems [5]. Detergents are amphiphilic molecules and remove the lipid surrounding the protein almost completely [6]. They form protein-detergent-lipid complexes (PDLC) containing the protein [7]. In figure 1.1 the whole process of solubilization of membrane proteins with detergents is depicted. Detergents are added to the sample until the critical micelle concentration (CMC) is reached. After adding it to a membrane preparation the micelles extract membrane proteins from the lipid bilayer, forming PDLCs [7].

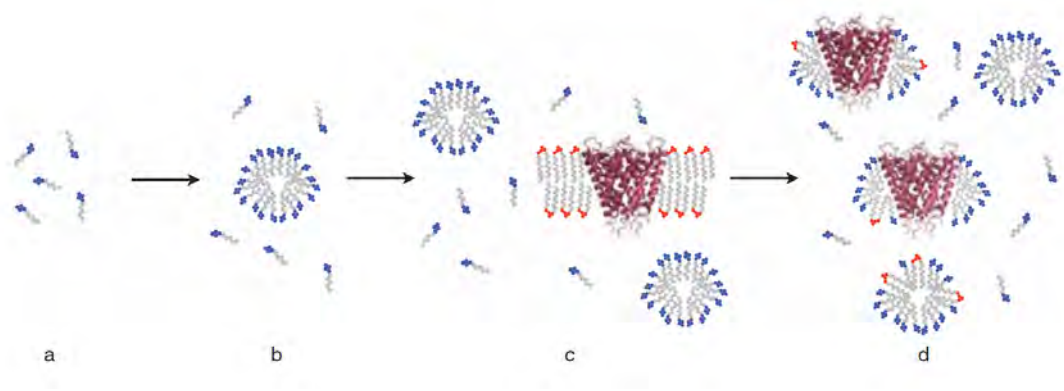

Figure 1.1: Detergent solubilization of membrane proteins. Free detergent monomers **a** associate to form micelles **b** at a concentration above the CMC. The micelles extract membrane proteins from the lipid bilayer **c** yielding a solution containing PDLCs, free lipid detergent micelles and detergent monomers **d**. Figure taken from [7] and edited.

Membrane proteins are susceptible to unfolding and aggregation when solubilized in detergents [8]. This may result in alteration of their native structure and a disruption in the biological function [9]. Therefore the proteins need to be reconstituted into artificial lipid systems, like Large Unilamellar Vesicles (LUVs) [10] or so called bicelles [11]. To achieve this goal, the detergent needs to be removed. The method of choice depends on the detergent. Detergents with a high CMC value are removed by dialysis [12]. Detergents with a low CMC value are adsorbed onto beads [10]. This whole process is labor intensive and bears a risk that the protein is not functional, since it is ripped of its native membrane surrounding [13].

1.2 Amphipols

Another way to extract membrane proteins from the cell are short amphiphilic polymers, so called amphipols. They adsorb tightly onto the hydrophobic part of the membrane protein and remove the surrounding lipid completely [14]. They increase the stability of membrane proteins in general. Furthermore, relatively low concentrations of amphipols are needed to solubilize a membrane protein, compared to detergents [15]. A major draw back is still the lack of lipid surrounding the proteins.

1.3 Nanodiscs

A novel approach is to incorporate membrane proteins into nanodiscs [16]. These nanodiscs contain the membrane protein in a lipid bilayer. The bilayer is surrounded by amphiphilic molecules like proteins [17, 18], peptides [19] or synthetic polymers. Two different approaches to form nanodiscs exist. The first one is to use so called membrane scaffold proteins (MSP), which were first introduced by [18]. However to incorporate membrane proteins, the use of detergent is still needed [20]. Since MSPs are not capable of dissolving a membrane. To reconstitute a protein into a nanodiscs stabilized with MSPs the cell membrane is solubilized with the detergent at the presence of MSPs. After removing the detergent a MSP-supported nanodisc is formed with the target protein incorporated in it [20]. In figure 1.2 the whole process is depicted.

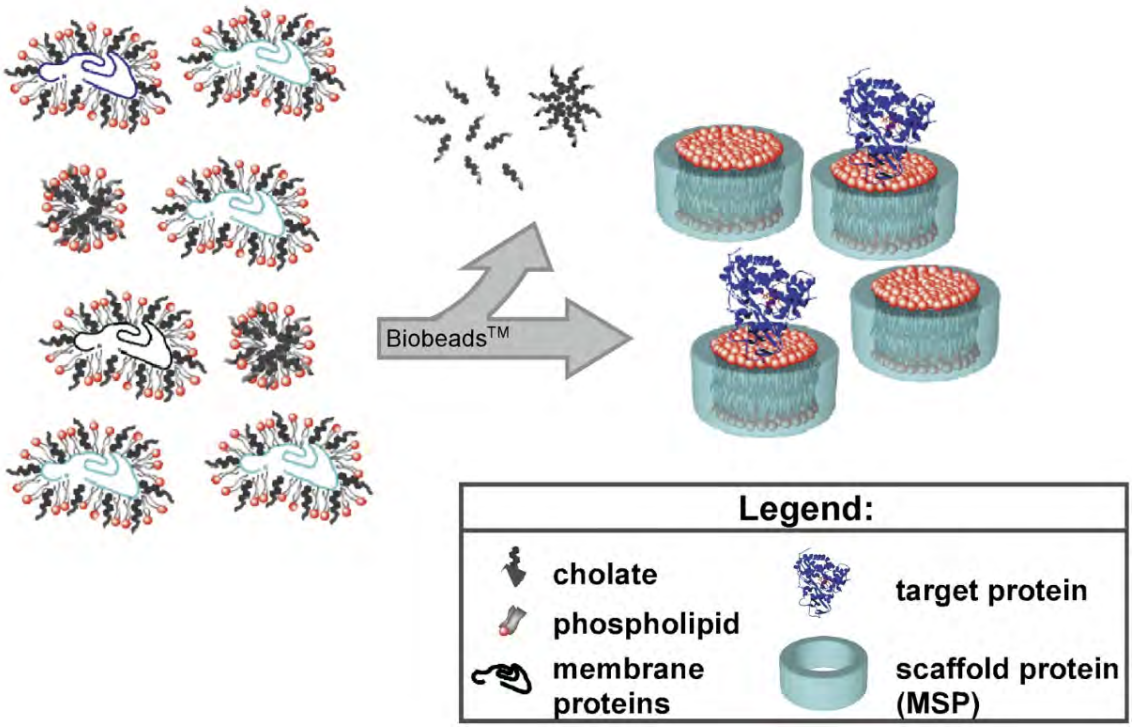

Figure 1.2: A cell membrane preparation containing the target membrane protein is solubilized with detergent in the presence of (MSPs). Upon removal of the detergent, by dialysis or Bio-Beads, a soluble MSP-supported nanodisc is formed with the target protein incorporated into the resulting phospholipid bilayer. Figure taken from [20].

The second approach is to directly dissolve the membrane with polymers. The advantage of this method is that these nanodiscs represent a more native environment compared to the convectional way of using detergent or amphipols. It has been shown that such an environment is essential for the function and stability fo membrane proteins [21]. Different polymers which are suitable to solubilize lipid membranes and incorporate membrane proteins into nanodiscs such as styrene-maleic acid (SMA) [22], diisobutylene-maleic acid (DIBMA) [23, 24] and glyco-diisobutylene-maleic acid (Glyco-DIBMA) [25] have been found. The different types of polymers will be discussed in section 2.1. Glyco-DIBMA (figure 2.2) is used in this work. All of these polymers have the ability to directly dissolve a cell membrane [23, 24, 25, 26] with the protein directly incorporated into nanodiscs. This of course has the advantage, that no reconstitution into artificial systems is needed and the protein is never stripped of its native lipid environment.

The membrane mimetic system explained above except of vesicles are shown in figure 1.3. Only the use of polymer nanodiscs ensures, that the protein is always surrounded by its native environment.

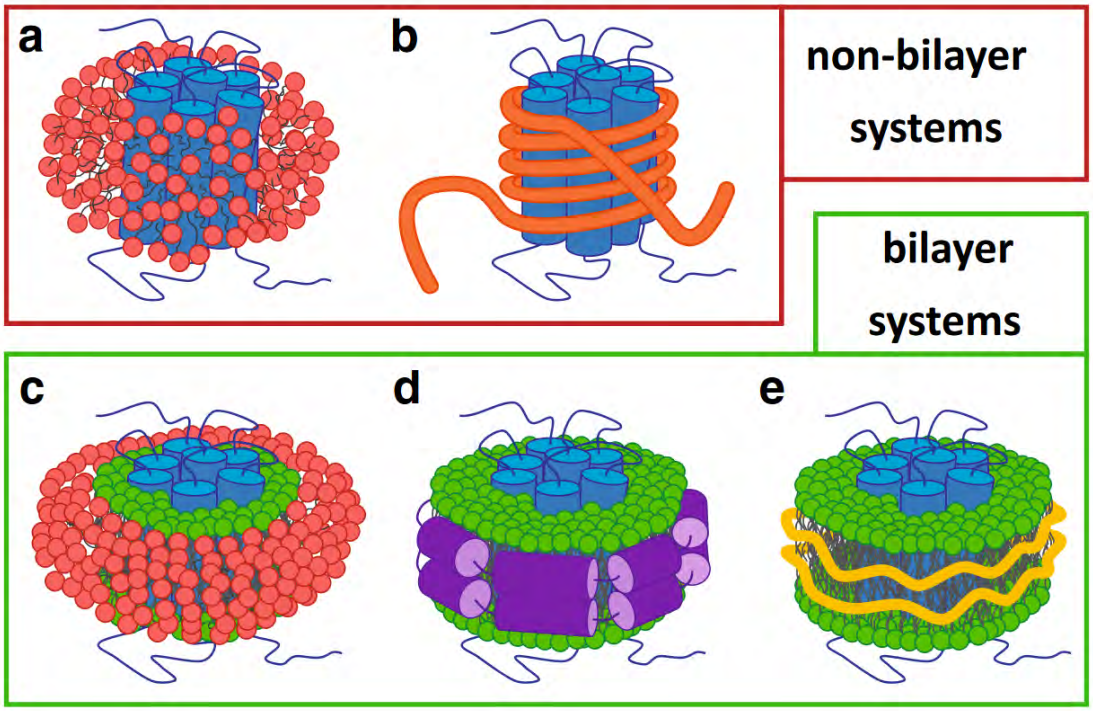

Figure 1.3: Membrane mimetic systems for membrane protein solubilization. The protein is displayed in blue the lipid in green. Panels in the red border are non bilayer systems, there is no lipid molecules around the protein. Panels in the green border are bilayer systems, there are lipid molecules around the protein. **a:** Protein in detergent (red) micelle. **b:** Protein stabilized by amphipol (orange). **c:** Protein in lipid detergent (red) bicelle. **d:** Protein in nanodisc stabilized by a protein (purple). **e:** Protein in nanodisc stabilized by a polymer (yellow). Figure taken from [15].

1.4 Goals

The main goals of this work are:

1. Preparation of L-α-PC polymer-nanodiscs.
2. Formation of Giant Unilamellar Vesicles (GUVs) containing lipids from polymer-nanodiscs
3. Reconstitution of a membrane protein, namely Gloeobacter Ligand-gated Ion Channel (GLIC) into polymer-nanodiscs.
4. Use protein-containing nanodiscs for protein reconstitution into GUVs.

2 Theory

In this chapter different polymers will be discussed and what advantages and disadvantages they have compared to each other. Furthermore a short insight in the formation of nanodiscs will be given. At last methods to control efficiency of extraction into nanodiscs will be discussed.

2.1 Polymers

Three polymers which are suitable for dissolving lipid bilayers and the formation of nanodiscs will be introduced in this section. A common one is SMA. It is displayed in figure 2.1 in panel **a** in the upper part. SMA consists of styrene, an aromat, and maleic acid. The capability of SMA to dissolve lipid bilayers and capture membrane proteins has been shown by various publications [27, 28, 29, 30, 15]. Furthermore, the insertion of a membrane protein into planar bilayers [26], as well as vesicles [31] has been achieved. However, SMA consists of styrene, which is an aromat, hence there is an absorption of ultraviolet (UV) light (see figure 2.1 panel **b**). This can become problematic, because some detection methods for proteins rely on UV absorption and can not be used accurately, if the polymer itself has a high absorbance at the desired wavelength.
Another suitable polymer is DIBMA. It is also shown in figure 2.1 in panel **a**. DIBMA does not contain an aromat, therefore the absorption in the UV range is smaller compared to SMA. In figure 2.1 in panel **b** the two absorption curves for different wavelengths are observable. The overall absorbance for DIBMA in the range of 230 nm - 320 nm is smaller. This brings the advantage that protein detection methods which rely on UV absorbance are accessible now. However, DIBMA has decreased lipid solubility, which is of course a drawback.

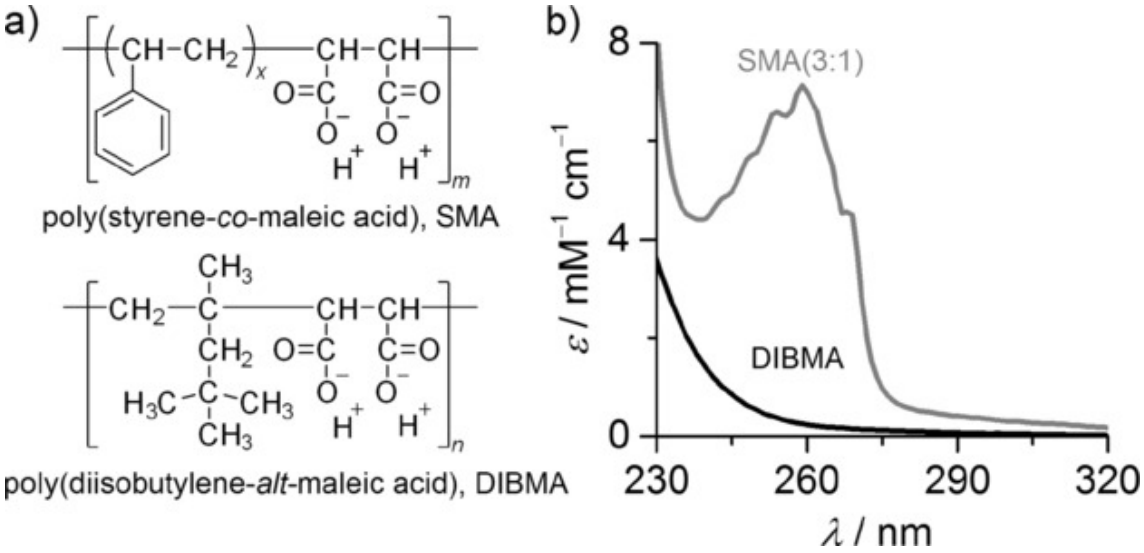

Figure 2.1: **a:** Chemical structures of SMA (3:1) (number average $m \approx 9$, $x \approx 3$, $M_n = 4.0\,\mathrm{kg\,mol^{-1}}$) and DIBMA (number average ≈ 37, $M_n = 8.4\,\mathrm{kg\,mol^{-1}}$). SMA (3:1) means that there are about 3 times more styrene molecules than maleic acid molecules ($x \approx 3$) **b:** Molar extinction coefficients ϵ of SMA (3:1) and DIBMA as functions of wavelength λ. Figure taken from [23]

Glyco-DIBMA (figure 2.2) presents an alternative to SMA and DIBMA. It has no aromatic ring as DIBMA and hence is suitable for UV absorption experiments. Moreover, the solubility of lipid bilayers is increased, compared to DIBMA.

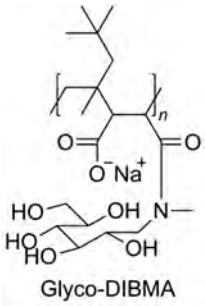

Figure 2.2: Schematic representation of Glyco-DIBMA taken from [25] and edited.

2.2 Nanodisc Formation

In this section the formation of nanodiscs is explained for the polymer SMA. The model is taken from [15] and describes the process of nanodiscs formation as a three-step model. In the first step SMA binds to the surface of the lipid bilayer. This process is modulated by the concentration of polymer, the present salt concentration and the presence of anionic lipid. Since SMA is negatively charged (figure 2.1), the presence of anionic lipid impairs the binding. Whereas an increased ionic strength promotes the binding of SMA. In the second step SMA inserts into the hydrophobic core of the membrane. This process is affected by the bilayer thickness and the lipid packing. The thicker the bilayer and tighter it is packed, the more the insertion of SMA is impaired. The last step is the complete solubilization into nanodiscs. If sufficient polymer is bound to the membrane, the kinetics mainly depend on the second step. An insertion into the hydrophobic core of the bilayer bears a large enthalpic penalty for the polar/charged carboxyl groups. Therefore, as soon as anionic SMA reaches the hydrophobic core of the bilayer, the formation of nanodiscs will occur. The process of nanodiscs formation with SMA is depicted in figure 2.3. For

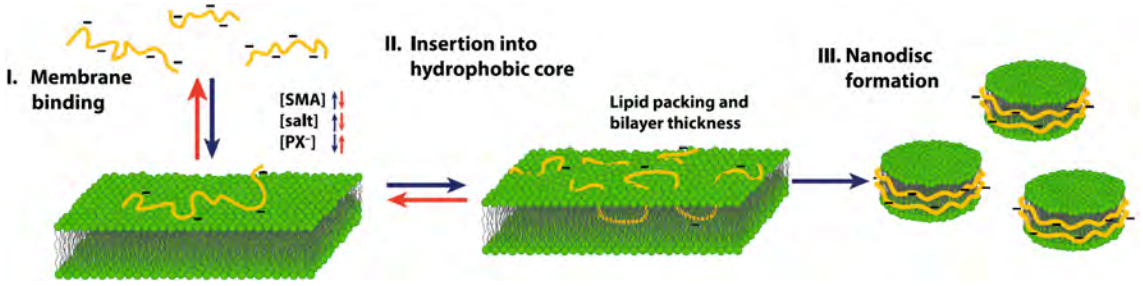

Figure 2.3: Schematic representation of nanodisc formation. The yellow string represents SMA with its negative charges. The lipid bilayer is schon in green. In the first step SMA binds to the membrane. This is driven by the concentration of polymer, salt and charged lipid head groups. In the second step SMA inserts itself into the hydrophobic core of the bilayer. The third step is the actual formation of nanodiscs. Figure taken from [15] and edited.

DIBMA and Glyco-DIBMA similar results are obtained. With an increasing concentration of polymer the diameter of nanodiscs gets smaller, however at a certain concentration a plateau is reached. Furthermore it is shown that not only the salt concentration has an impact on the formation of nanodiscs but the pH as well. For DIBMA an increased ionic strength facilitates the formation of nanodiscs. For Glyco-DIBMA however this result is not observed. Anionic lipids hamper the formation of nanodiscs with DIBMA, as it is

stated for SMA. Since Glyco-DIBMA has a lower charge density compared to DIBMA the effect of anionic lipid is less high as compared to DIBMA. Not only the presence of negatively charged lipids modulates the formation of nanodiscs, but the acyl chain length and the saturation as well. For DIBMA an increasing acyl length and unsaturation is unfavorable for the formation of nanodiscs [25, 24, 23]. In a negative-stain transmission electron microscope (TEM) experiment it is shown that LUVs out of 1,2-dimyristoyl-sn-glycero-3-phosphocholine (DMPC), which are solubilised with DIBMA at a mol fraction of $\frac{c_{DIBMA}}{c_{DMPC}} = 0.10$ form actual disc shaped particles [23]. 1-palmitoyl-2-oleoyl-sn-glycero-3-phosphocholine (POPC) and DMPC vesicles are mixed with Glyco-DIBMA to a polymer lipid mass ratio of 1.5 and 2 respectively. TEM experiments show the formation of disc shaped particles [25]. A similar result is obtained for SMA. POPC vesicles and SMA are mixed at a weight ratio of 1:1.5 respectively. TEM shows the formation of disc shaped particles [32].

2.3 Measuring Size and Number of Nanodiscs

In this section the diffusion of a sphere and a disc through a viscous liquid at low reynolds numbers will be introduced.

2.3.1 Hydrodynamic Radius of a Sphere

In figure 2.4 a sphere falling through a liquid is depicted. The acting forces are gravity F_g, which pulls the sphere down and stokes drag F_d which counteract on F_g. The force of a viscous fluid on a spherical particle is given by the so called Stoke's drag [34][35]:

$$F_d = 6\pi\eta R_s v = \zeta v \tag{2.1}$$

Where η is the dynamic viscosity of the fluid, R_s is the radius of the spherical object and v is flow velocity relative to the object. ζ is called the drag coefficient. The diffusion coefficient D is known as [36]:

$$D = \frac{k_b T}{\zeta} \tag{2.2}$$

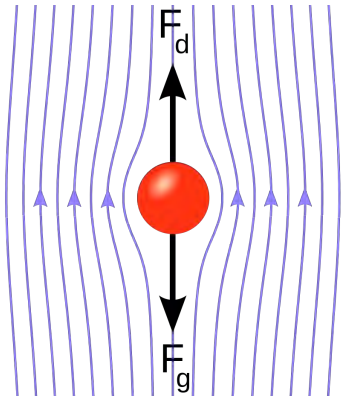

Figure 2.4: Schematic representation of a sphere in red falling through a liquid. In blue the streamlines. F_g is the gravity force which pulls the sphere down. F_d is the stokes drag which counteracts gravity. Figure taken from [33].

Where k_b is Boltzmann's constant and T the absolute temperature. By combining equation 2.1 and 2.2 one gets:

$$D = \frac{k_b T}{6\pi\eta R_s} \tag{2.3}$$

By rearranging equation 2.3 one gets the so called hydrodynamic radius of a sphere:

$$R_s = \frac{k_b T}{6\pi\eta D} \tag{2.4}$$

2.3.2 Hydrodynamic Radius of a Disc

The drag coefficient ζ of a disc moving due to Brownian motion through a liquid with viscosity η can be written as [37]:

$$\zeta = 12\eta R_d \tag{2.5}$$

Where R_d is the radius of the disc. Hence the hydrodynamic radius of a disc can be written as:

$$R_d = \frac{k_b T}{12\eta D} \tag{2.6}$$

Equations 2.5 and 2.6 only hold for actual 2D particles. Nanodiscs of course have height and are therefore more like flat cylinders then actual discs. The thickness of a lipid bilayer depends on the acyl chain length [38]. Molecular simulations indicates a bilayer thickness for E.Coli of (38.15 ± 0.03) Å [39] and (38.67 ± 0.07) Å [40]. However, there

are no analytical solutions for a cylinder moving at random through a viscous liquid. Therefore the simplified approach of a two dimensional discs is used.

3 Materials and Methods

3.1 Nanodiscs from Large Unilamellar Vesicles

LUVs are prepared with L-α-PC from soybean Type IV-S. Atto 655 DPPE is a lipid dye. This dye is added to 0.0002 m% to observe the sample with fluorescence correlation spectroscopy (FCS) (section 3.4). The lipid with the dye is dissolved in buffer to a concentration of 5 mg mL^{-1} and vortexed until all of the lipid is completely dissolved. This procedure results in so called Multilamellar Vesicles (MLVs). MLVs, LUVs and Small Unilamellar Vesicles (SUVs) are depicted in figure 3.1.

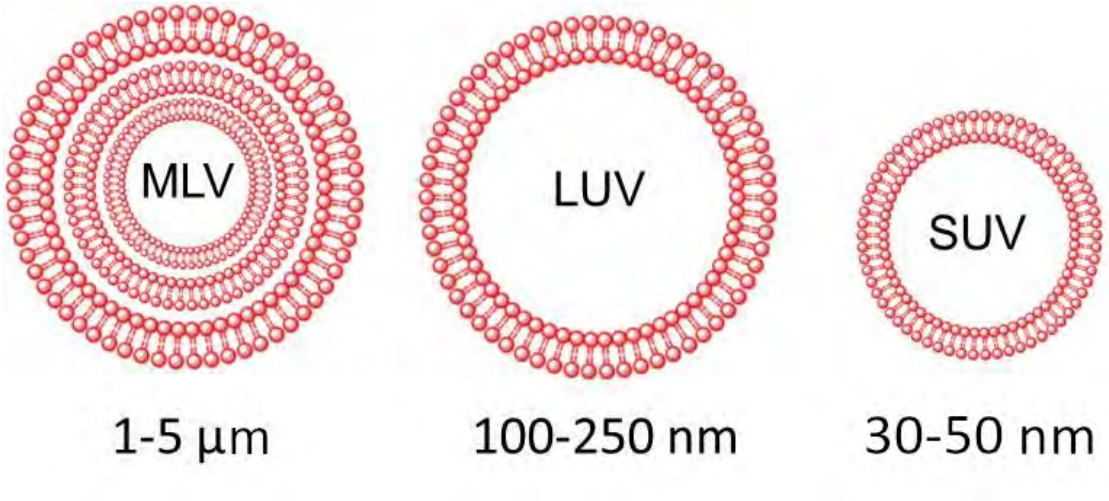

Figure 3.1: This figure shows the difference between MLVs, LUVs and SUVs. As shown the MLV contains multiple bilayers, whereas the LUV and the SUV just have one bilayer. The difference between the LUV and the SUV is only in size. The diameter of each vesicle is written beneath each image. Figure taken from [41] and edited.

MLVs have multiple bilayers whereas LUVs have just one. To get LUVs from MLVs the suspension containing the MLVs is extruded through a 200 nm filter. This procedure results

in LUVs with approximately 200 nm in diameter. Glyco-DIBMA, DIBMA or Mcb120n is added to a mass ratio of various concentrations (section 4.1). The suspension is incubated over night at room temperature. The whole process results in nanodiscs of different sizes depending on the added polymer concentration.

3.2 Nanodiscs Incorporation into Giant Unilamellar Vesicles

The protocol of [42] is used and adapted to produce GUVs. Glasslides are coated with 1 % w/v of agarose and dried for 1 h at 55 °C in an oven at atmospheric pressure. MLVs out of 2,3-Di-O-phytanyl-sn-glycero-1-phosphocholine (DPHPC) (figure 3.2) with 0.01 m% Atto 488 DPPE and 0.000 05 m% Atto 633 DPPE, which are both lipid dyes, are prepared as described in the section above to a concentration of $3\,\mathrm{mg\,mL^{-1}}$. A low salt buffer containing 5 mM KCl, 2 mM Trehalose and 1 mM HEPES is used. The pH of the buffer is adjusted to 7.4. To get SUVs from MLVs the suspension is sonificated until the turbidity is significantly reduced.

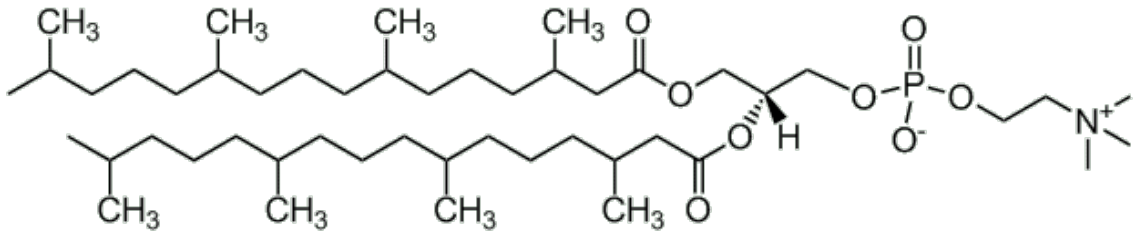

Figure 3.2: Structure of the lipid DPHPC. From [43]

SUVs and Nanodiscs with 0.1 m% Atto 633 DPPE are mixed to a mass ratio of 1:10 of L-α-PC to DPHPC. This results in a 1:1 ratio of Atto 633 DPPE from nanodiscs to Atto 488 DPPE from SUVs. Around 60 µL of the suspension is spreaded on the agarose glassslide and put into a vacuum desiccator for 1 h to partially dehydrate the solution. 1 mL of a growth buffer containing 5 mM KCl, 400 mM Sucrose and 1 mM HEPES is put on the glassslide. The buffer is adjusted to pH 7.4. The slides are put into a fridge and rehydrated for 2 h at 4 °C. GUVs will swell out of the lipid film.

The whole process of gel-assisted swelling is depicted in figure 3.3.

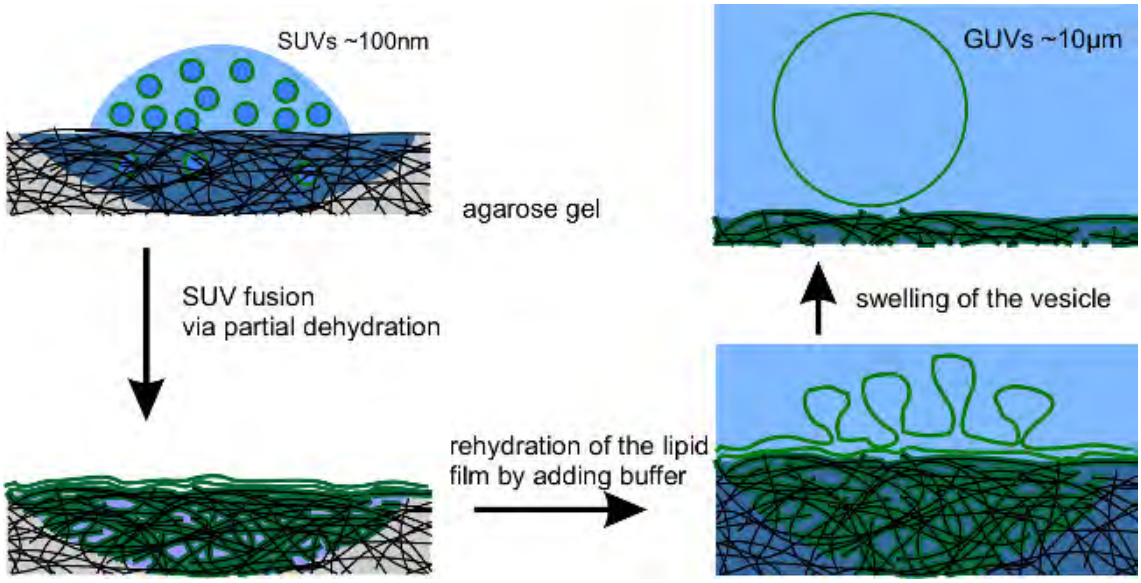

Figure 3.3: This figure shows the whole process of gel-assisted swelling of GUVs. A solution (light blue) containing SUVs (dark blue with a green lipid bilayer) is spread onto an a glassslide coated with an agarose gel (black lines). The solution is partially dehydrated. The buffer evaporates and a lipid film sticks onto the agarose gel. The film is rehydrated and GUVs (green circle) swell out of the lipid film. Figure taken and adapted from [42].

3.3 Protein Purification

The membrane protein GLIC is purified after the following protocol. The media, buffer and stock solutions which are used, are displayed in table 3.1 and table 3.2.

First of all an overnight culture is made. Therefore LB-Medium and 100 µg mL^{-1} kanamycine are put into a flask together with the cells. Kanamycine is an antibiotic which the cells are resistant against. Hence all other bacteria will be killed. The whole sample is incubated over night at 37 °C with $\sim$ 160 rpm. The overnight culture as well as 100 µg mL^{-1} kanamycine are put into 1 L LB-Medium in a 2 L flask. The mixture is incubated at 37 °C with 150 rpm and grown until $OD_{600} \sim 0.8$. OD stands for optical density and 600 stands for the wavelength of the light in nm. To measure OD_{600} 1 mL of sample is pipetted into a cuvette. A spectrometer shines light with a wavelength of 600 nm on it. The light

will be scattered and absorbed by the sample. The scattered light is measured as the OD value. After OD_{600} reaches 0.8 the protein production is induced by 0.25 mM IPTG and the sample is incubated over night at 20 °C with 150 rpm. IPTG stands for Isopropyl β-D-1-thiogalactopyranoside which removes a repressor on the lac operon to induce gene expression. The cells are harvested by centrifugation of the sample at 4 °C with 5000 g for 20 min. The supernatant is autoclave waste. The remaining cell pellet can be put into a tube and stored in a freezer or further processed. The frozen pellet is thawed and then resuspended in lysis buffer. The mixture of pellet and buffer is homogenized three times with an *Emulsiflex-C5* from *AVESTIN*. The homogenized solution is centrifugated at 4 °C with 6000 g for 15 min. The supernatant is put under ultracentrifugation at 4 °C with 100 000 g for 1 h. Supernatant can be thrown away. The remaining membrane fraction is weighed and resuspended in standard buffer to a concentration of 100 mg ml^{-1}. It can be stored in a freezer.The membrane fraction and Glyco-DIBMA (figure 2.2) are mixed to a mass ratio of 1:1. The mixture is put under agitation over night at 4 °C. The suspension is ultracentrifugated with 100 000 g at 4 °C for 1 h. The supernatant contains the solubilised proteins.

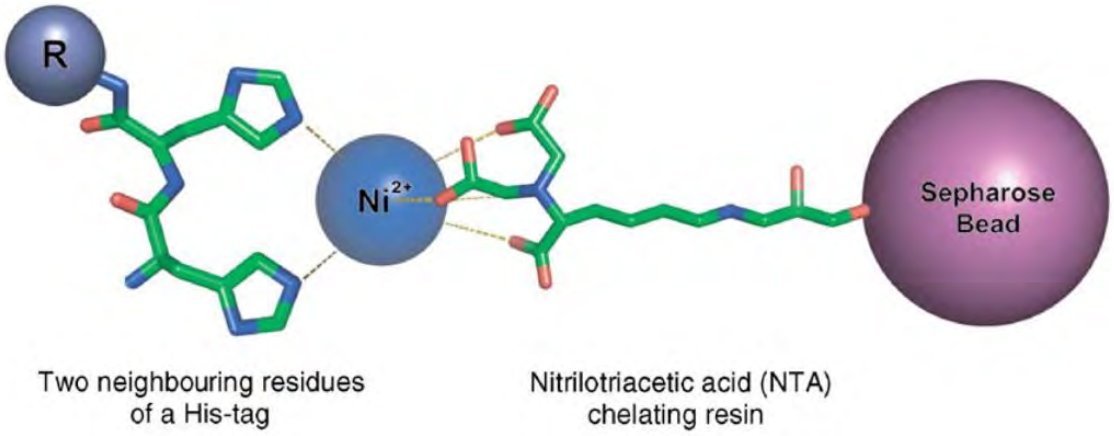

Figure 3.4: Schematic picture of a NTA resin with a N^{2+} ion bound to it and a protein (R) with to histidines also bound to it. The NTA occupies 4 binding sites of the N^{2+} and the histidines 2 binding sites. Figure taken from [44] and adapted.

The proteins are purified with nickel affinity chromatography and labeled with a fluorescent dye. The schematic mechanism of nickel affinity chromatography is depicted in figure 3.4. A His-tag (multiple Histidines) are covalently bound to the protein. Nitrilotracetic acid (NTA) is bound on a sepharose bead. This whole NTA complex occupies only four

out of six binding sites to a Ni^{2+} ion. The other two can be occupied by two histidines. Hence only the protein of interest, which is labeled with a His-tag, will stay on the column. All other proteins will be washed away. To eluate the wanted protein from the column a buffer with a high imidazole (figure 3.5) concentration is used. Imidazole mimics histidine and competes for binding to the beads.

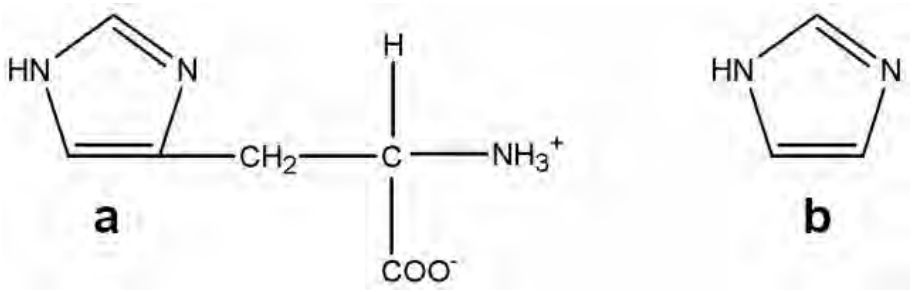

Figure 3.5: **a:** The structure of the amino acid histidine. **b:** The structure of imidazole on the right side. Figure taken from [45] and edited.

1 ml of nickel resin is put in to a column. It is washed with water and standard buffer. The solubilised proteins are put into the column and incubated over night under agitation at 4 °C. Then washed with wash buffer. Tris (2-carboxyethyl) phosphine (TCEP) is added and incubated with the sample for 15 min. TCEP breaks disulfide bonds which are needed for labeling. TCEP is washed away and a suited maleimide dye is added. The sample is incubated for 1 h at room temperature to ensure the binding of the dye onto the target protein. The process of the binding of the dye is depicted in figure 3.7. A fluorescent molecule is attached to a maleimide molecule. The maleimide molecule binds covalently to a thiol group. To ensure a thiol group exists a point mutation to a cysteine (figure 3.6) is carried out on the desired place. Then the dye is washed away with wash buffer and the sample eluated with the elution buffer.

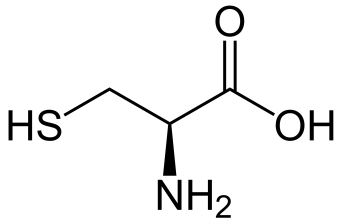

Figure 3.6: Structure of L-Cysteine. Cysteine is the only amino acid which contains a thiol group. Figure taken from [46].

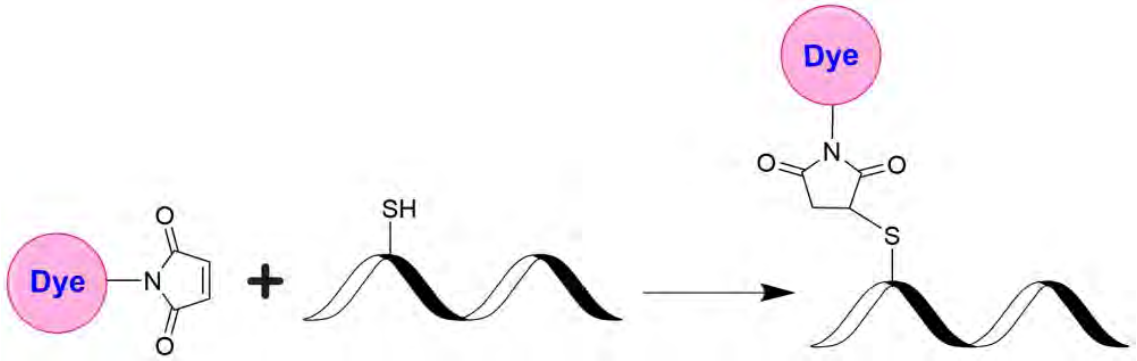

Figure 3.7: Process of the binding of an maleimide molecule with a dye to a thiol group. Figure taken from [47] and adapted.

LB-Medium	
$10\,g\,l^{-1}$	trypton
$5\,g\,l^{-1}$	yeast extract
$10\,g\,l^{-1}$	NaCl
	pH 7.2

Table 3.1: Used medium for overnight culture and cell culture

Buffers	
standard buffer	50 mM Tris, 150 mM NaCl, pH 7.4
lysis buffer	standard buffer + c0mplete
washing buffer	standard buffer + 25 mM imidazole
elution buffer	standard buffer + 500 mM imidazole

Table 3.2: Used buffers for the purification

3.4 Fluorescence Correlation Spectroscopy

The underlying principle of fluorescence correlation spectroscopy (FCS) is confocal microscopy. The principle of confocal microscopy is depicted in figure 3.8. A laser is focused through an objective onto a sample. The fluorescence light is collected by the same objective and is imaged through an emission filter and a lens onto a pinhole. This pinhole blocks light which does not originate from the confocal volume. The resolution in z direction is enhanced compared to conventional microscopes. Light which passes the pinhole is collected by a detector.

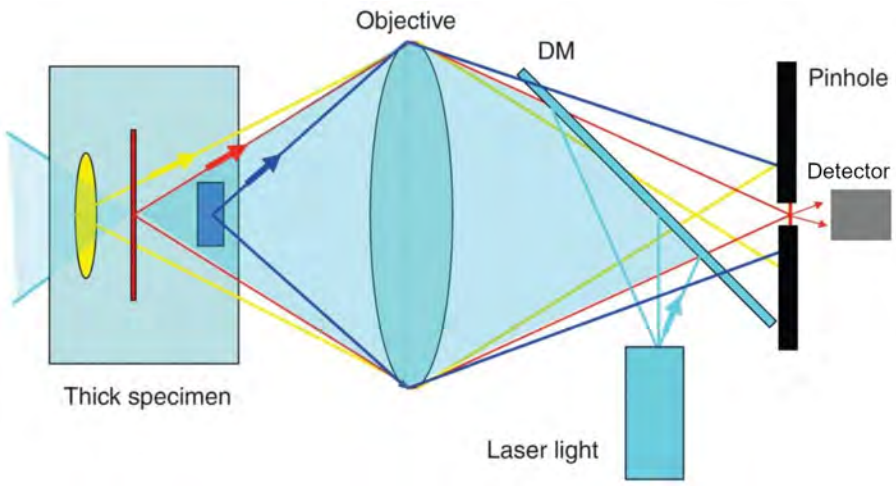

Figure 3.8: Schematic setup of a laser scanning confocal microscope. Laser light is focused through an objective and a dichroic mirror (DM) onto a sample (specimen). The fluorescence light from the sample is collected by the same objective and imaged on a pinhole. Light which does not originate from the focal plane is cut of. The light which passes the pinhole is collected by a detector. Figure taken from [48] and adapted.

In a FCS setup (figure 3.9) a laser beam is focused through an objective onto the sample. The sample gets illuminated and the fluorescence of the sample is collected by the same objective. After passing a dichroic mirror and an emission filter the light is focused through a lens on a pinhole, which blocks the fluorescent light not originating from the focal region. After the pinhole a detector detects the signal. [49]

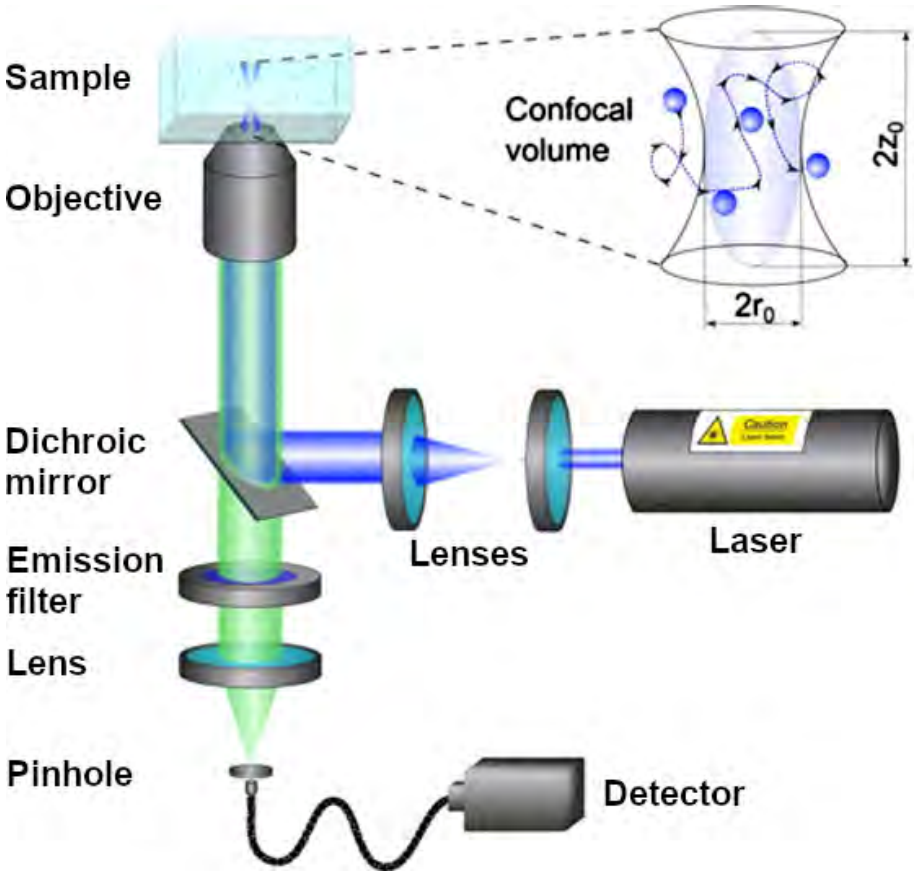

Figure 3.9: Schematic representation of a confocal FCS setup. A laser beam is focused on the sample. The excited fluorescence light is collected by the same objective. After passing through a dichroic mirror and an mission filter it is imaged onto a confocal pinhole, to block light which is out of focus. After the pinhole the light is imaged on a detector. Figure taken from [49] and adapted.

The signal collected by the detector $F(t)$ is autocorrelated with itself. In figure 3.10 an example trace from a low concentration (A) and a high concentration (B) sample with their corresponding autocorrelation functions is depicted. The autocorrelation function is defined as:

$$G(\tau) = 1 + \frac{\langle \delta F(t) \delta F(t+\tau) \rangle}{\langle \delta F(t) \rangle^2} \tag{3.1}$$

Where $F(t)$ is the collected fluorescence signal, $\delta F(t) = F(t) - \langle F(t) \rangle$. $\langle\rangle$ denotes the time average. If the the fluorescence is only caused by the diffusion of an identical ensemble of particles the autocorrelation function can also be written as [50]:

$$G(\tau) = 1 + \frac{1}{N} G_D(\tau) \tag{3.2}$$

Where

$$G_D(\tau) = \left(1 + \frac{\tau}{\tau_D}\right)^{-1} \left(1 + \frac{r_0^2 \tau}{z_0^2 \tau_D}\right)^{-\frac{1}{2}} \tag{3.3}$$

N is the average number of fluorescent particle in the excitation volume, τ_D is the diffusion time, r_0 is the width of the confocal volume and z_0 the height of the volume. The obtained autocorrelation function (equation 3.1) from the measurement is fitted with the analytical solution (equation 3.2). Since the confocal volume V_{eff} is known one can obtain the particle concentration from:

$$N = \frac{1}{G(0) - 1} \tag{3.4}$$

The diffusion coefficient can be calculated from the diffusion time τ_D with the following relation [50]:

$$D = \frac{r_0^2}{4\tau_D} \tag{3.5}$$

Figure 3.10 illustrates how the signal and the autocorrelation curve change for different conditions. In A a single particle, hence low concentration, is diffusing through the confocal volume. An example fluorescent trace is displayed next to it as well as the corresponding autocorrelation function. It is indicated in the sketch that with slower diffusion the curve is shifted to the right. Hence the diffusion time τ_D increases. It is directly proportional to the width of the autocorrelation curve. In B multiple particles are diffusing through the confocal volume. The fluorescence trace shows a higher intensity compared to A, but the amplitude of the correlation curve is shifted downwards with a higher concentration. The concentration is indirectly proportional to the height of the amplitude of the autocorrelation curve.

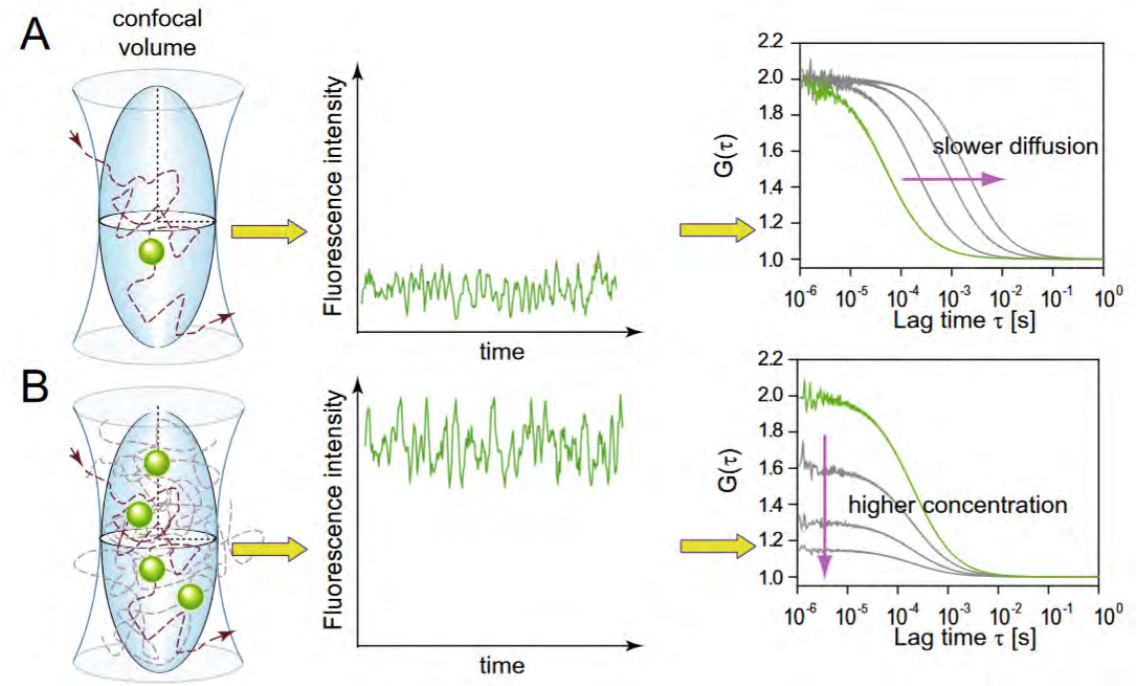

Figure 3.10: Schematic representation of a confocal FCS measurement. In A a low concentration sample diffusing through the confocal volume is depicted together with the corresponding fluorescence trace and its autocorrelation function. In B a sample with a high concentration is depicted together with the corresponding fluorescence trace and its autocorrelation function. Figure taken from [51] and adapted.

Fluorescent molecules are exited from a ground state S_0 to an excited state S_1. Both of these states are singlet states. If the molecule converts to ground state again, fluorescence occurs. However, it is also possible for the molecule to reach a long lived triplet state T_1 after excitation. In this triplet state the molecule stops fluorescing. In figure 3.11 the three states are depicted with their rate constants k_{ij}.

k_{12} is the rate constant for exiting the molecule from S_0 to S_1. k_{21} denotes the rate constant for fluorescence. k_{23} is the rate constant for entering the triplet state and k_{31} is the rate constant from triplet state to ground state. If this process is accounted for, the autocorrelation function can be written as [50]:

$$G(\tau) = 1 + \frac{1}{N}\left(1 + \frac{T}{1-T}\exp\left(-\frac{\tau}{\tau_T}\right)\right) G_D(\tau) \tag{3.6}$$

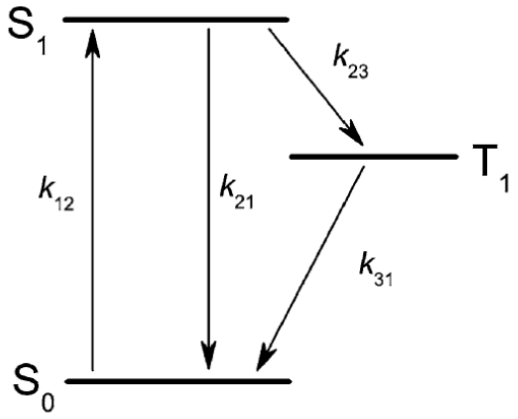

Figure 3.11: Simplified Jabłoński diagram, with the ground state S_0, the excited state S_1 , the triplet state T_1 and the corresponding rate constants. Figure taken from [50] and adapted.

Where N is the number of fluorescent particles in the observation volume, T is the fractional population of the triplet state in the observation volume, τ_T is the triplet state blinking time, G_D is the correlation function for free diffusion (see equation 3.3).

3.5 Single Molecule Fluorescence Microscopy

The Single Molecule Fluorescence Microscope (SMFM) is a simple inverted microscope where the sample can be either illuminated with white light, a polychrome and three different lasers. The lasers have either a wavelength of 640 nm, 532 nm or 488 nm. A scheme of the setup can be seen in figure 3.12. The laser light is guided through different

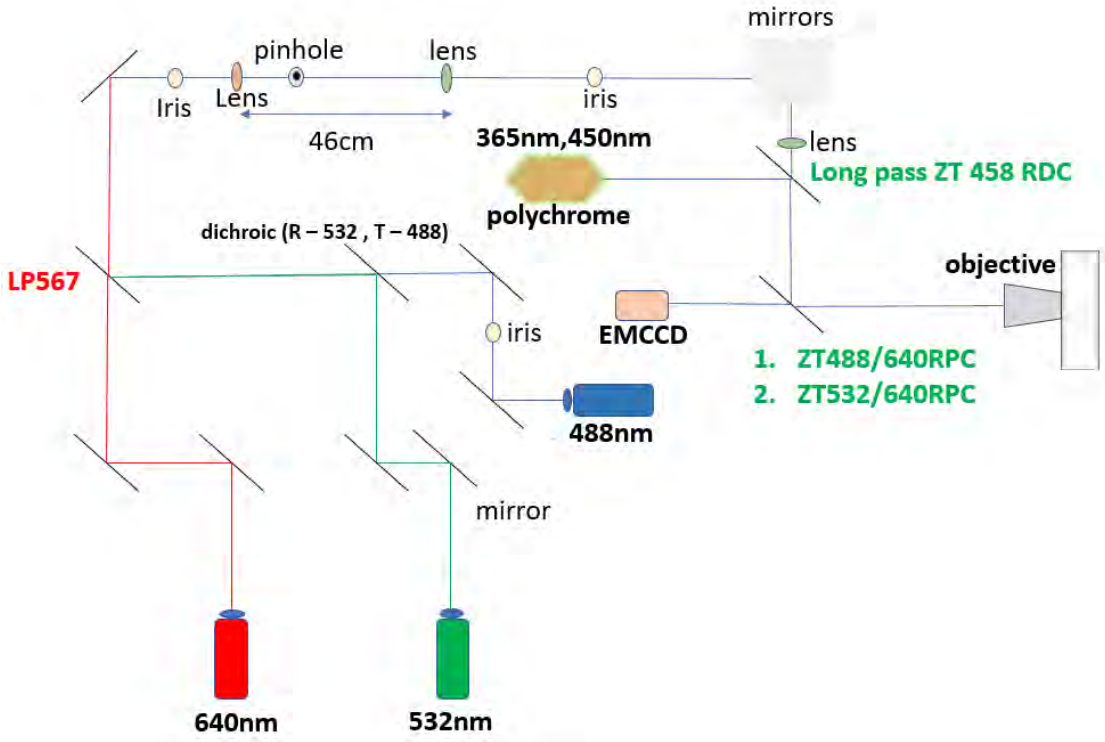

Figure 3.12: Schematic representation of the SMFM setup. Mirrors indicated as lines are simple mirrors, which just reflect the laser light. The mirrors displayed as block also includes some lenses to focus the laser. Figure kindly provided from Rohit Yadav.

lenses and pinholes and projected on the objective. As well as collected with a electron multiplying charge-coupled device (EMCCD) and imaged on a camera.

4 Results and Discussion

4.1 Nanodiscs out of LUVs

LUVs are produced as described in 3.1. DIBMA, Mcb120n and Glyco-DIBMA are added to the LUV suspension. DIBMA and Mcb120n are added to the following mass concentration fractions $\frac{c_p}{c_l} = 0$, $\frac{c_p}{c_l} = 2.2$, $\frac{c_p}{c_l} = 4.5$ and $\frac{c_p}{c_l} = 11.2$. Glyco-DIMBA is added to the following mass concentration fractions $\frac{c_p}{c_l} = 0$, $\frac{c_p}{c_l} = 1.1$, $\frac{c_p}{c_l} = 2.2$ and $\frac{c_p}{c_l} = 11.2$. c_p denotes the mass concentration of polymer and c_l the mass concentration of lipid. To check if nanodiscs have formed, the sample is measured via FCS (section 3.4). Figures 4.1, 4.2 and 4.3 show the measured autocorrelation curves. With the values from the fitting parameters the tables 4.1, 4.1 and 4.1 are obtained. The diffusion coefficients are calculated with equation 3.5. Set parameters, which are independent from the fits are V_c=$8 \cdot 10^{-16}$ L, r_0=265 nm, k_b=$1.38 \cdot 10^{-23}$ J K^{-1}, T=297 K and η=$1 \cdot 10^{-3}$ Pa s. Where V_c is the confocal volume, r_0 is the radius of the confocal volume, k_b is Boltzmann's constant, T is the absolute temperature and η is the viscosity of water.

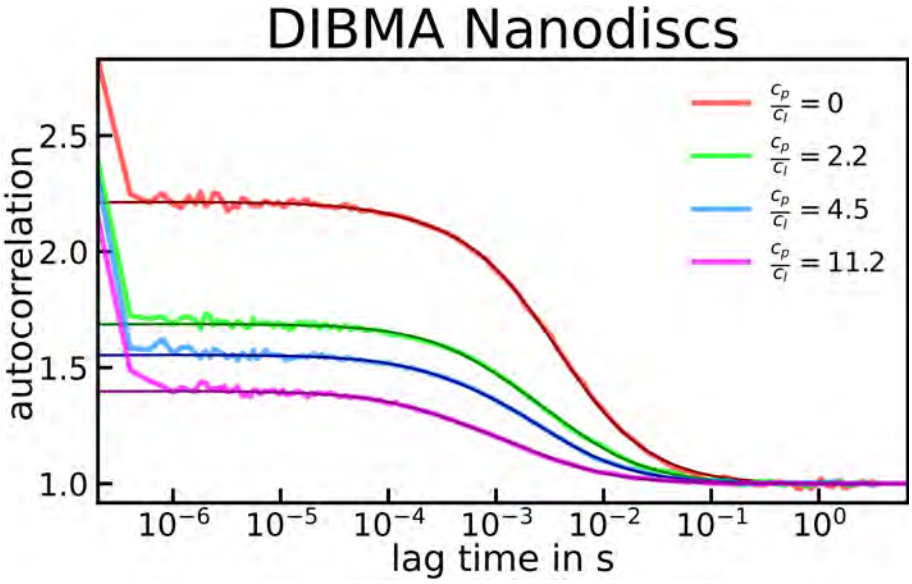

Figure 4.1: Plot of the correlation functions and the corresponding fits for different concentration ratios of lipid to DIBMA. Red corresponds to $\frac{c_p}{c_l} = 0$, green to $\frac{c_p}{c_l} = 2.2$, blue to $\frac{c_p}{c_l} = 4.5$ and purple to $\frac{c_p}{c_l} = 11.2$. The lag time in seconds is plotted on the x-axis. The autocorrelation function is plotted on the y-axis.

The autocorrelation curve in 4.1 is fitted with equation 3.6. The hydrodynamic radius in table 4.1 is calculated with equation 2.4.

$\frac{c_p}{c_l}$	τ_D in µs	N	c in nM	D in $\mathrm{cm^2\,s^{-1}}$	R_0 in nm
0	3645	0.8	1.7	$4.8 \cdot 10^{-8}$	44.9
2.2	3586	1.7	3.4	$4.9 \cdot 10^{-8}$	44.1
4.5	2579	2.0	4.0	$6.8 \cdot 10^{-8}$	31.7
11.2	1752	3.1	6.3	$1 \cdot 10^{-7}$	21.6

Table 4.1: This table shows the diffusion time τ_D from the fit in figure 4.1, the number of particles N form the fit in 4.1, the calculated concentration c, the calculated diffusion coefficient D and the hydrodynamic radius R_0 for different DIBMA to lipid mass fractions.

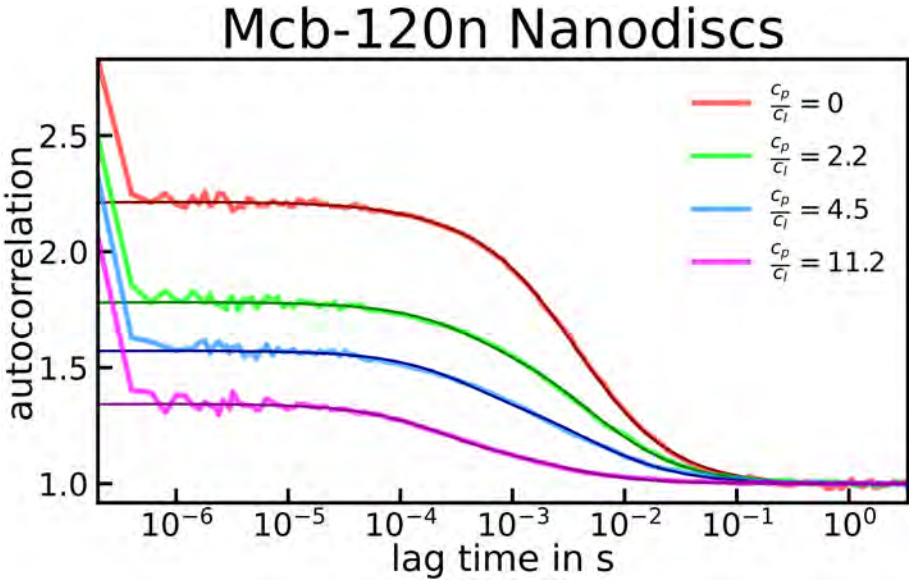

Figure 4.2: Plot of the correlation functions and the corresponding fits for different concentration ratios of lipid to Mcb120n. Red corresponds to $\frac{c_p}{c_l} = 0$, green to $\frac{c_p}{c_l} = 2.2$, blue to $\frac{c_p}{c_l} = 4.4$ and purple to $\frac{c_p}{c_l} = 11.2$. The lag time in seconds is plotted on the x-axis. The autocorrelation function is plotted on the y-axis.

The autocorrelation curve in 4.2 is fitted with equation 3.6. The hydrodynamic radius in table 4.1 is calculated with equation 2.4.

$\frac{c_p}{c_l}$	τ_D in µs	N	c in nM	D in $\mathrm{cm^2\,s^{-1}}$	R_0 in nm
0	3645	0.8	1.7	$4.8 \cdot 10^{-8}$	44.9
2.2	4515	1.5	3.1	$3.9 \cdot 10^{-8}$	55.6
4.5	4213	2.4	4.9	$4.2 \cdot 10^{-8}$	51.9
11.2	1502	4.9	9.8	$1.2 \cdot 10^{-7}$	18.5

Table 4.2: This table shows the diffusion time τ_D from the fit in figure 4.2, the number of particles N form the fit in 4.2, the calculated concentration c, the calculated diffusion coefficient D and the hydrodynamic radius R_0 for different Mcb120n to lipid mass fractions.

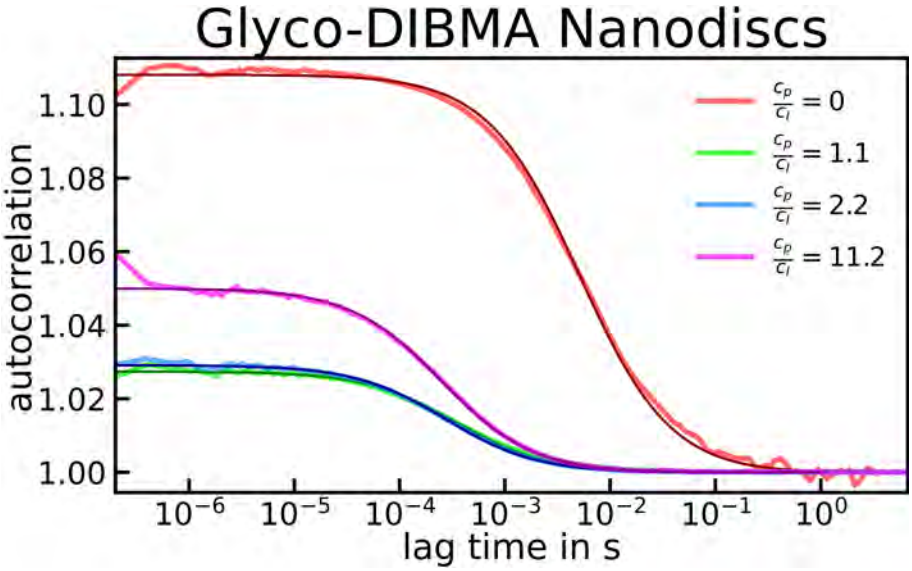

Figure 4.3: Plot of the correlation functions and the corresponding fits for different concentration ratios of lipid to Glyco-DIBMA. Red corresponds to $\frac{c_p}{c_l} = 0$, green to $\frac{c_p}{c_l} = 1.1$, blue to $\frac{c_p}{c_l} = 2.2$ and purple to $\frac{c_p}{c_l} = 11.2$. The lag time in seconds is plotted on the x-axis. The autocorrelation function is plotted on the y-axis.

Equation 3.2 was used to fit the autocorrelation curve in figure 4.3. For $\frac{c_p}{c_l} = 0$. Equation 2.4 has been used to calculate the hydrodynamic radius R_0, since the LUVs can be assumed to be spherical. Whereas for all other ratios equation 2.6 was used to calculate the hydrodynamic radius, since these particles can be assumed to be disc shaped.

$\frac{c_p}{c_l}$	τ_D in µs	N	c in nM	D in $\mathrm{cm^2\,s^{-1}}$	R_0 in nm
0	5116	9	18	$3 \cdot 10^{-8}$	62.6
1.1	346	36	73	$5 \cdot 10^{-7}$	6.6
2.2	275	34	69	$6 \cdot 10^{-7}$	5.3
11.2	251	20	40	$7 \cdot 10^{-7}$	4.8

Table 4.3: This table shows the diffusion time τ_D from the fit in figure 4.3, the Number of particles N form the fit in 4.3, the calculated concentration c, the calculated diffusion coefficient D and the hydrodynamic radius R_0 for different Glyco-DIBMA to lipid mass fractions.

As it can be seen in tables 4.1, 4.1 and 4.1 with an increasing amount of the corresponding polymer the particle size decreases. However only for Glyco-DIBMA it is obvious that nanodiscs have formed. Furthermore smaller amounts of Glyco-DIBMA is needed to form nanodiscs, compared to the other polymers. The difference between DIBMA and

Mcb-120n is small. For $\frac{c_p}{c_l} = 11.2$ the measured size difference for these two polymers is only 3.1nm. For Glyco-DIBMA no significant reduction between the mass fraction $\frac{c_p}{c_l} = 2.2$ to $\frac{c_p}{c_l} = 11.2$ is observable. Dynamic light scattering (DLS) measurements of DMPC LUVs mixed with DIBMA, yield a similar result. However, DIBMA nanodiscs seem to be larger, with a diameter of 20 nm under similar conditions [23, 24]. Glyco-DIBMA seem to produce smaller nanodiscs as it is shown in this experiment as well as in DLS experiments [25]. The DLS experiments show that Glyco-DIBMA do not only produce smaller nanodiscs, diameter around 10 nm, but also the sizedistribution of the nanodiscs is smaller. SMA produces nanodiscs at almost the same diameter ((13 ± 6) nm) [52] as Glyco-DIBMA. The sharp increase in concentration from $\frac{c_p}{c_l} = 0$ to $\frac{c_p}{c_l} = 1.1$ can be explained by the solubilization of LUVs into nanodiscs. One LUV is dissolved into multiple nanodiscs, hence the concentration increases. The decrease of the concentration from $\frac{c_p}{c_l} = 1.1$ to $\frac{c_p}{c_l} = 11.2$ might be explained by the greater dilution of the sample due to the higher titration volumes of the Glyco-DIBMA stock. The radius of 62.2 , seems inline with literature [53, 54] for a poresize of 200 nm. Overall the experiment seems to be inline with the literature and furthermore provides an alternative method (FCS) to determine the radius of nanodiscs. Since in the cited literature above only DLS is used to determine the size of the nanodiscs. From this experiments it can be concluded that only Glyco-DIBMA produces nanodiscs with a small radius at low polymer concentrations.

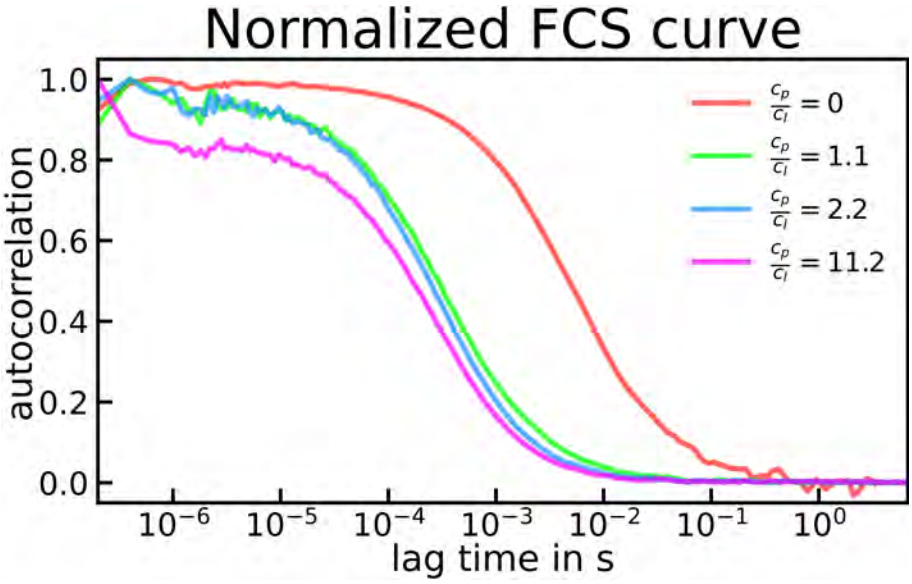

Figure 4.4: Plot of the normalized correlation functions without fits for Glyco-DIBMA (figure 4.3). Red corresponds to $\frac{c_p}{c_l} = 0$, green to $\frac{c_p}{c_l} = 1.1$, blue to $\frac{c_p}{c_l} = 2.2$ and purple to $\frac{c_p}{c_l} = 11.2$. The lag time in seconds is plotted on the x-axis. The autocorrelation function is plotted on the y-axis.

4.2 Lipid Nanodiscs Incorporation into GUVs

GUVs with and without nanodiscs are produced as described in section 3.2. GUVs from SUVs with 0.01 m% Atto 488 DPPE and 0.000 05 m% Atto 633 DPPE are prepared as a control. GUVS from SUVs with 0.01 m% Atto 488 DPPE and 0.000 05 m% Atto 633 DPPE as well as nanodiscs with 0.1 m% Atto 633 DPPE are prepared, to check if nanodiscs incorporation into GUVs is possible. The GUVs are checked in a Single Molecule Fluorescence Microscope (section 3.5). A glassslide is coated with 5 mg ml betacasein, which passivate the glass, to ensure that GUVs do not adhere, spread and rupture on the chamber surface [42]. 500 µL of an observation buffer, which contains 100 mM KCl, 200 mM Glucose and 20 mM Tris. The pH is adjusted to 7.5. 5 µL of the GUV sample are put into the observation buffer. The whole sample is put onto the objective of the microscope. The results of this experiment are shown below. In figure 4.5 a GUV without nanodiscs is shown in white light. In figure 4.6 a GUV without nanodiscs is shown in blue light (left part of the image) and red light (right part of the image). The laser power for the blue laser (wavelength

of 488 nm) is 1 mW. The power for the red laser (wavelength of 640 nm) is 25 mW. The exposure time for both wavelengths is 50 ms.

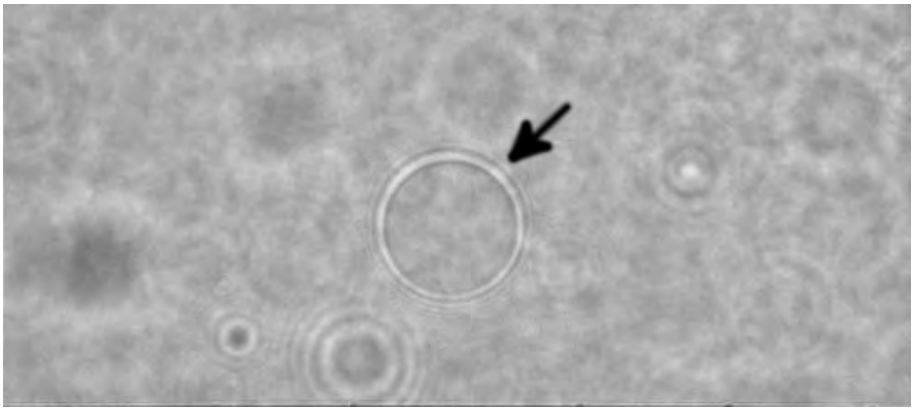

Figure 4.5: Control GUV in white light. The black arrow indicates the GUV

The figures 4.5 and 4.6 show the expected result. There is a strong fluorescence in the blue channel, from Atto 488 DPPE and basically no fluorescence in the red channel, since there is such a small amount (0.000 05 m%) of Atto 633 DPPE. Although the laser power is significantly higher in the red channel compared to the blue one, there is still no significant fluorescence observable.

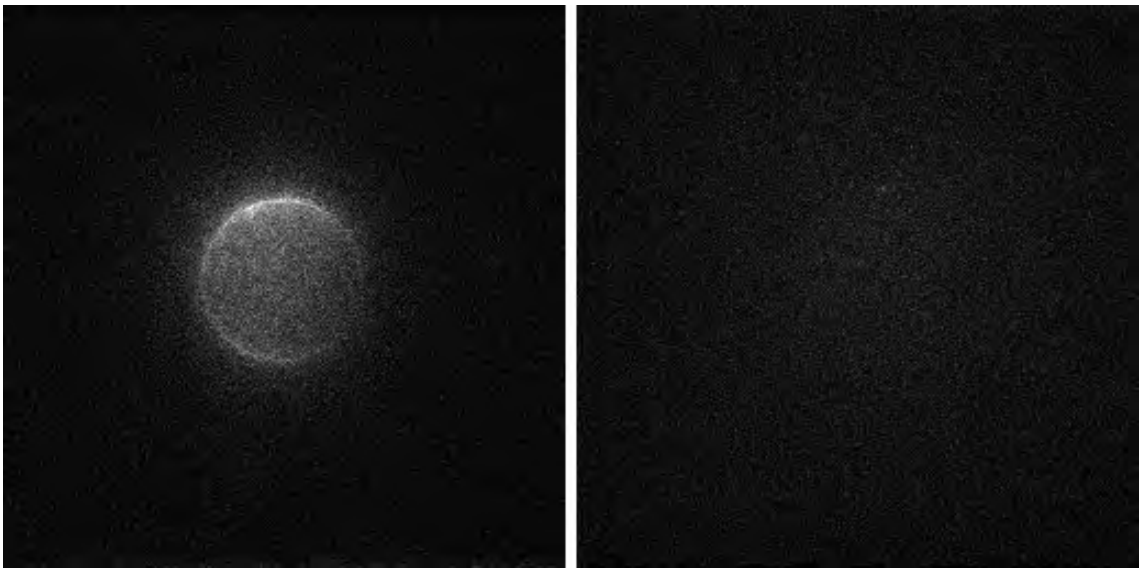

Figure 4.6: Control GUV in blue light and red light. The left part of the image corresponds to the blue laser. The excitation wavelength of the blue laser is 488 nm. The power of the blue laser is 1 mW. The right part of the image corresponds to the red laser. The excitation wavelength of the red laser is 640 nm. The power of the red laser is 25 mW. The exposure time for both images is 50 ms.

Then GUVs which are made out of SUVs and nanodiscs are observed. The set power of the blue laser is 1 mW and the exposure time is 50 ms. These are the same settings, as for the GUV without nanodiscs. For the red laser however the power has been significantly reduced from 25 mW to 0.5 mW. The exposure time is the same, namely 50 ms. The figures 4.7 and 4.8 show the results. Figure 4.7 shows a GUV made out of SUVs and nanodiscs in white light. In figure 4.8 a GUV out of SUVS and nanodiscs exposed to blue and red light is displayed.

The laser power of the red laser in the control sample with GUVs without nanodiscs (figure 4.8) is significantly reduced compared to the red laser power in the sample with GUVs with nanodisc (figure 4.6). However, the fluorescence in the red channel is increased a lot compared to the control experiment. The blue fluorescence is high in both samples. There is almost no fluorescence in the control sample, although the laser power is high. This is expected, since there is only little amount (0.000 05 m% Atto 633 DPPE) red dye in the sample. Whereas there is a high red fluorescence in the sample with nanodiscs. Since only the nanodiscs are labeled with a high amount (0.1 m%) of red dye and mixed with a

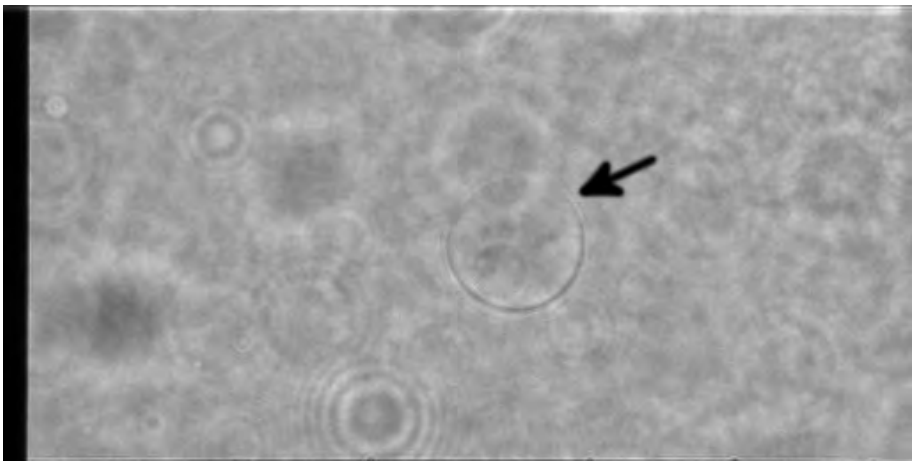

Figure 4.7: GUV out of SUVs and nanodiscs in white light. The black arrow indicates the GUV.

lipid ratio of 1:10 of nanodiscs to SUVs it can be concluded that the fluorescence in the red channel in figure 4.8 comes from nanodiscs and they indeed incorporated into GUVs.

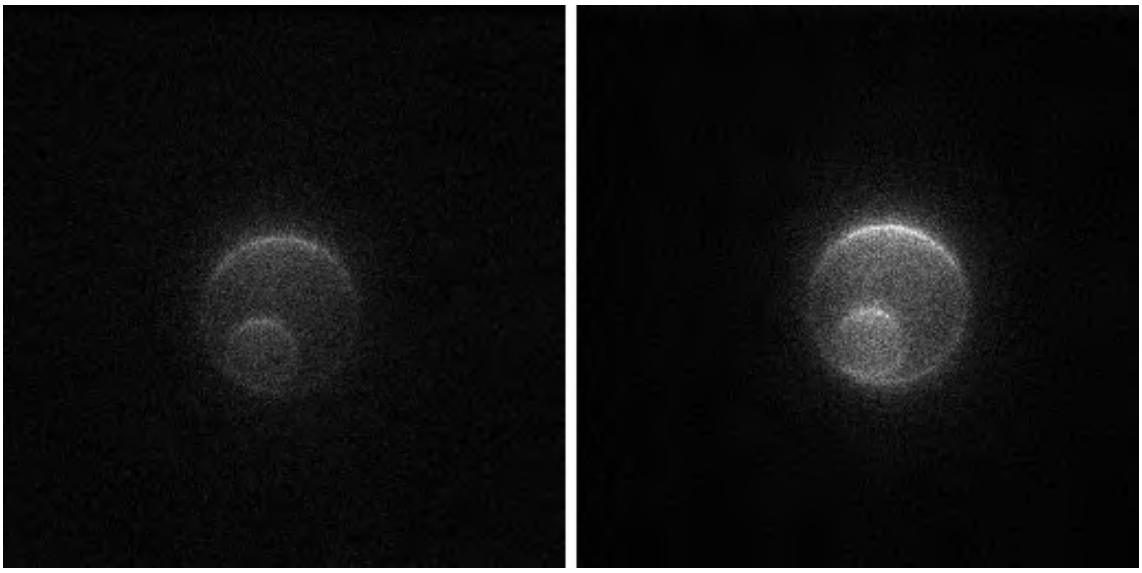

Figure 4.8: GUV out of SUVs and nanodiscs in blue light and red light. The left part of the image corresponds to the blue laser. The excitation wavelength of the blue laser is 488 nm. The power of the blue laser is 1 mW. The right part of the image corresponds to the red laser. The excitation wavelength of the red laser is 640 nm. The power of the red laser is 0.5 mW. The exposure time for both images is 50 ms.

In general the yield of GUVs is low in the sample and also aggregates appeared in the sample. An aggregate is shown in white light in figure 4.9 and in blue and red light in figure 4.10. The low yield of GUVs and the occurrence of aggregates could be explained, by the presence of Glyco-DIBMA in the sample. In successful reconstitutions of protein nanodiscs into LUVs Mg^{2+} is used to get rid of SMA [31]. Although Glyco-DIMBA is used and not SMA the approach of using Mg^{2+} could still be worth a try.

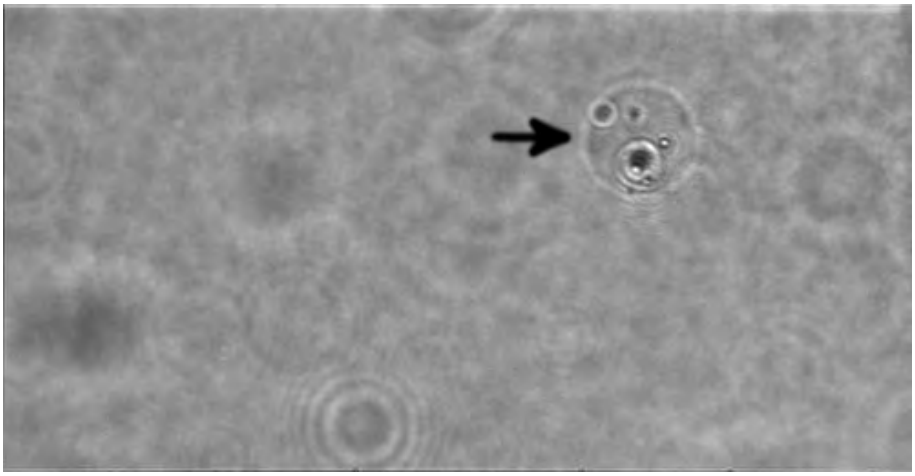

Figure 4.9: Aggregate in white light. The black arrow indicates the aggregate.

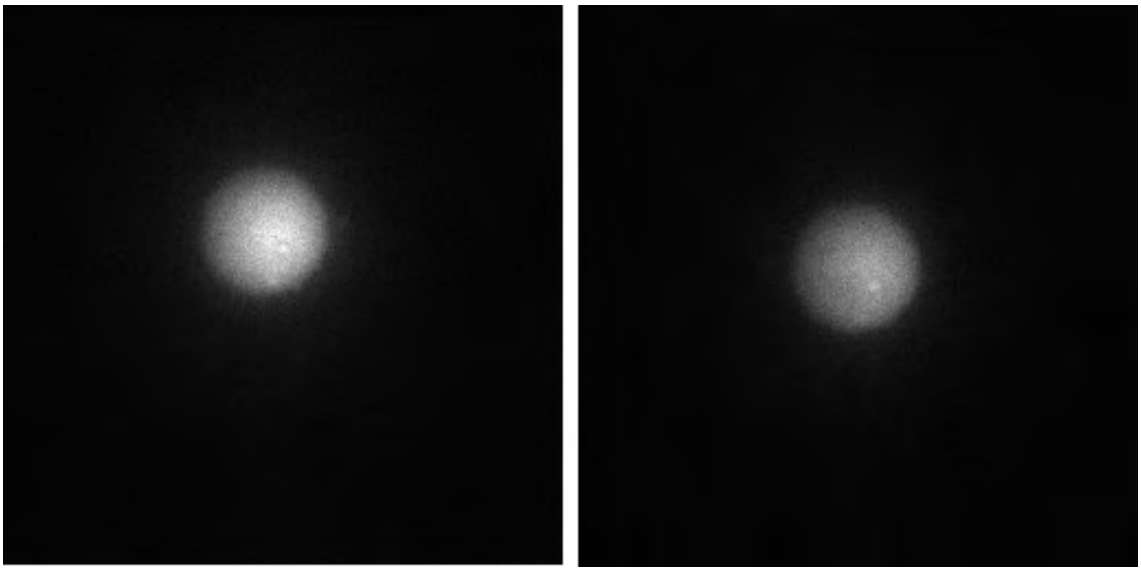

Figure 4.10: Aggregate in blue light on the left side. Same aggregate in red light on the right side.

4.3 Protein Reconstitution into Nanodiscs

The membrane Protein GLIC is reconstituted as described in section 4.3. The protein is labeled with Alexa Fluor 647 maleimide dye. The sample is measured via FCS the recorded curve with fit is shown below (Figure 4.11).

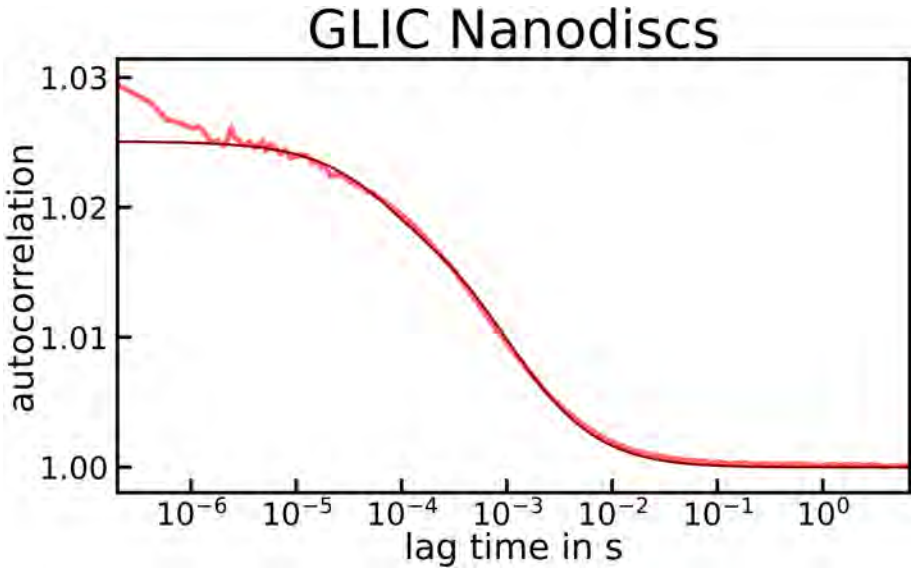

Figure 4.11: Plot of the autocorrelation functions and the corresponding fit for the labeled GLIC in Nanodiscs. A triplet state fit was used. The lag time in seconds is plotted on the x-axis. The autocorrelation function is plotted on the y-axis.

The obtained parameters from the fit and the resulting values are displayed in table 4.3. To calculate the diffusion coefficient the triplet state is taken into account and equation 3.5 is used. To calculate the hydrodynamic radius 2.6 is used.

τ_D in µs	N	c in nM	D in $\mathrm{cm^2\,s^{-1}}$	R_0 in nm
1006	51	102	$2 \cdot 10^{-7}$	19.4

Table 4.4: This table shows the diffusion time τ_D from the fit in figure 4.11, the number of particles N form the fit in 4.3, the calculated concentration c, the calculated diffusion coefficient D and the hydrodynamic radius R_0.

The radius of nanodiscs with the protein is about 3 times higher compared to nanodisc which purely consists out of lipid (tables 4.1 and 4.3). In an experiment where proteoliposomes are dissolved into nanodsiscs with the aid of DIBMA as well as pure liposomes no

difference in size between the 2 types of nanodiscs is observed [23]. However, the lipid composition has an impact on the solubility of the used polymer [23, 24, 25, 52]. Further experiments need to be carried out to really make sure the size difference is due to the lipid composition.
In the above experiment (section 4.2) lipid nanodiscs are incorporated into GUVs, the lipid mass ratio of nanodisc to SUVs is 1:10. The lipid concentration of the nanodiscs with GLIC needs to be estimated to have an insight about how much of the nanodiscs with GLIC sample has to be mixed with the SUVs. In the following paragraph the calculations to estimate the lipid concentration of the sample are shown. Fist of all the area of the disc is calculated. The area of the discs is 1181.8 nm^2, calculated from the hydrodynamic radius R_0. To estimate the area of lipid particles the area of the the protein needs to be subtracted. Therefore PyMOL is used to measure the diameter of GLIC. In the figure 4.12 below screenshots from PyMOL can be seen. The left panel shows the whole protein. The right panel shows a topview on the transmembrane part of the protein and its diameter.

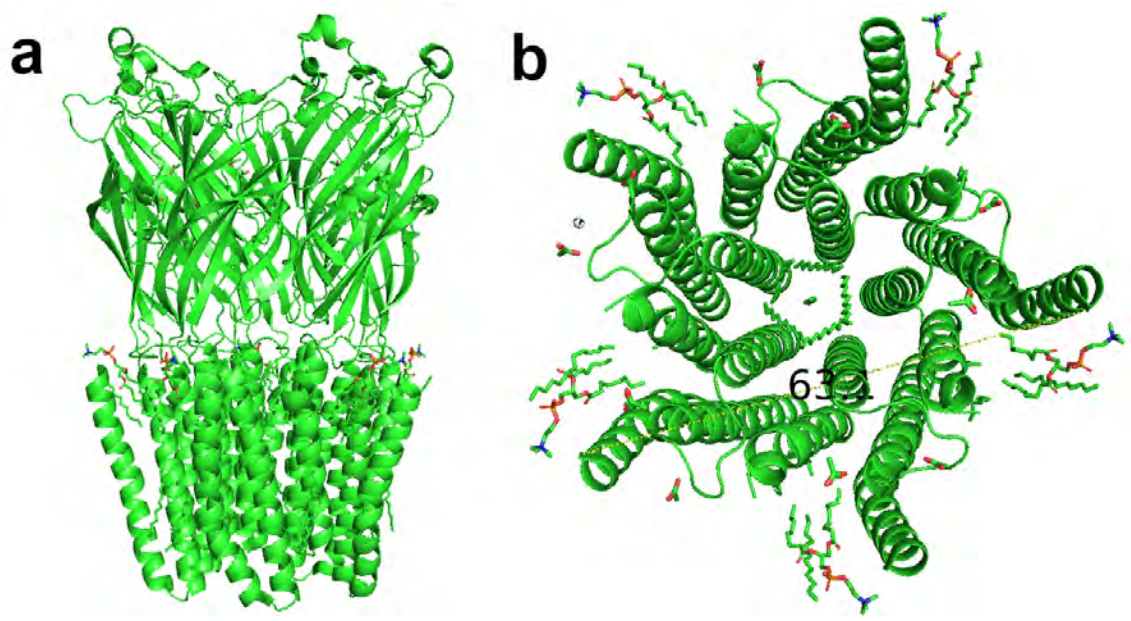

Figure 4.12: X-ray structure of the GLIC protein. The picture is a exported from PyMOL. The PDB-file is taken from [55]. **a:** the protein is displayed in side view. GLIC is a pentameric channel. Each subunit has four helices, where helix tow is forming th pore. The periplasmic part is on top of the membrane part. **b:** a plan view on th transmembrane part of the protein is shown. The distance calculated in PyMOL is 63.1 Å and can be seen as yellow dashed line.

In figure 4.12 it can be seen that the diameter is 63.1 Å. Hence the area of the protein is 31.3 nm^2. The area of the protein is subtracted from the whole area of a nanodisc to end up with the area that is occupied by lipids. This area is 1150.5 nm^2. Up to 80 % of the composition of *E. Coli* phospholipids is Phosphatidylethanolamine (PE) [56]. The surface area of EggPE is (71.4 ± 4.4) $Å^2$ [57]. Since nanodiscs are bilayer systems the area of lipid has to be multiplied by 2 before dividing it by the surface area of the lipid. The result is 3577 ± 136 lipid molecules per disc. The concentration of nanodiscs is 102 nM (from table 4.3). Therefore the concentration of lipid is (365 ± 14) µM. The molecular weight of a PE lipid from Avanti Polar lipid is 744.03 $g\,mol^{-1}$ [58]. This gives a lipid mass concentration of (0.27 ± 0.01) $mg\,mL^{-1}$. This calculation assumes that only nanodiscs with a protein are present in the sample and that all of these proteins are sufficiently labeled. Furthermore, it should be noted that not all phospholipids in E. Coli are PEs [56]. Hence to calculate the concentration assuming only PEs bears room for errors. It is unlikely that the used surface area and the molecular weight perfectly matches the present lipids. Therefore the calculated value might deviate from the real one, but to estimate the order of magnitude it should be sufficient. The mass concentration of lipid is needed to prepare proper GUVs. In section 4.2 it is noted that the mass concentration of nanodiscs to SUVs is 1:10. That is why the above calculation is carried out to obtain the lipid mass concentration and to proceed with the preparation of GUVs from SUVs and protein nanodiscs. This process is described in the next section (4.4).

4.4 Protein Nanodiscs Incorporation into GUVs

GUVs with protein nanodiscs are produced as described in section 3.2. SUVs contain 0.01 m% Atto 488 DPPE are mixed with GLIC nanodiscs to a lipid mass ratio of 1:20 of nanodiscs to SUVs. The protein is labeled with Alexa Fluor 647. The GUVs are checked in a Single Molecule Fluorescence Microscope (section 3.5).

In figure 4.13 a GUV with GLIC nanodiscs is shown in white light. In the next picture (figure 4.14) snapshots from a video at different times are displayed. The left part of the images is illuminated with a blue laser (wavelength 488 nm) at a power of 2 mW. The right part of the images is illuminated with a red laser (wavelength 640 nm) at a power of 6.4 mW. The exposure time is 50 ms and the frame rate of the video was 12 frames per second. Figure 4.14a is a snapshot of the GUV at 0 s. The fluorescence of the GUV in blue

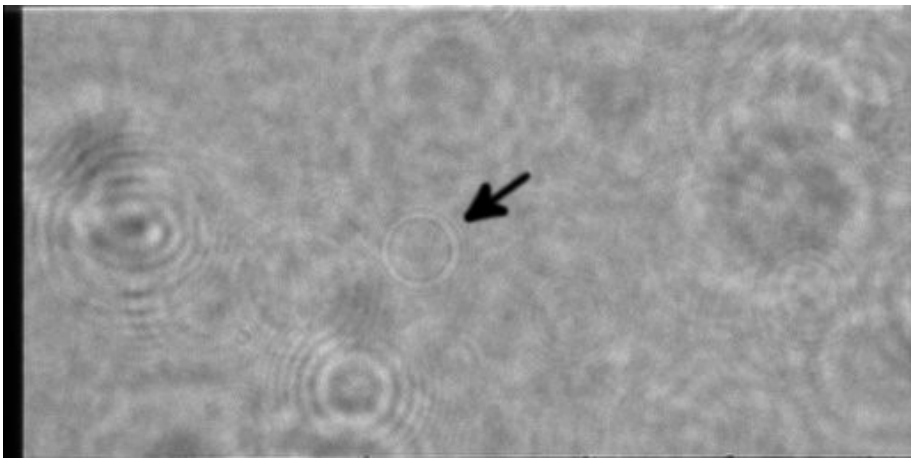

Figure 4.13: GUV out of SUVs and nanodiscs in white light. The black arrow indicates the GUV.

light is bright. Comparable to the GUV out of SUVs and the GUV out of nanodiscs and SUVs in section 4.2. The brightness in the red channel is really low, although the power of the red laser is higher than the power of the blue laser. Nevertheless a fluorescence in the red channel is observable, which indicates that some GLIC molecules are reconstituted into the GUV. Figure 4.14b is a snapshot of the GUV at 1 s. The image is really similar to figure 4.14a, where the GUV was captured at 0 s. Also here the GUV in the red channel is really faint, whereas the fluorescence in the blue channel is quite bright. The low fluorescence from the red dye indicates a low amount of protein in the GUV. Figure 4.14c is a snapshot of the GUV at 4 s. Compared tho the images above figure 4.14a and figure 4.14b, the brightness of the GUV in the red channel significantly decreased. It is almost non existent anymore, whereas the GUV in the blue channel is still clearly visible. Figure 4.14d is a snapshot of the GUV at 35 s. There is no GUV observable anymore in the red channel, whereas the blue channel still shows a lot of fluorescence. The red dye is completely bleached, but also the blue fluorescence is less bright compared to the image at 0 s (figure 4.14a). The yield of GUVs in this experiment is even lower than in the experiment where only lipid nanodiscs are incorporated into GUVs (section 4.2). Also the GUVs are smaller in size. This is observable from figure 4.8 and figure 4.14. The objective is the same in both figures, but the GUV from protein nanodiscs is smaller in size. The low yield of GUVs and there small size might be explainable due to the presence of Glyco-DIBMA in the sample. Also here the approach of using Mg^{2+} to get rid of Glyco-DIBMA might be useful. Furthermore in the nanodiscs with protein are present in the elution buffer which contains

50 mM Tris, 150 mM NaCl and 500 mM imidazole at a pH of 7.4. The estimated lipid concentration of the nanodiscs sample is $(0.27 \pm 0.01)\,\mathrm{mg\,mL^{-1}}$ (section 4.3). The lipid concentration of the SUVs is $3\,\mathrm{mg\,mL^{-1}}$ (section 3.2). For a lipid ratio of 1:20 the volume of nanodisc sample is $V_2 = 0.56 \cdot V_1$, where V_2 is the volume of nanodisc sample and V_1 is the volume of SUV sample. A mixture of the low salt buffer and the elution buffer in this ratio, will result in a buffer that contains 3.2 mM KCl, 1.3 mM Tris, 0.0 mM HEPES, 53.8 mM NaCl, 17.9 mM Tris and 179.5 mM imidazole. This is of course no low salt buffer anymore, but for the formation of GUVs a low salt buffer is required [42]. Therefore the low amount of GUVs and there small size might be explained by the missing of a low salt buffer. To tackle the problem the amount of nanodiscs could be decreases. However, the amount of protein is already low in the present GUVs. Another method would be for example to exchange the buffer via dialysis to a low salt buffer.

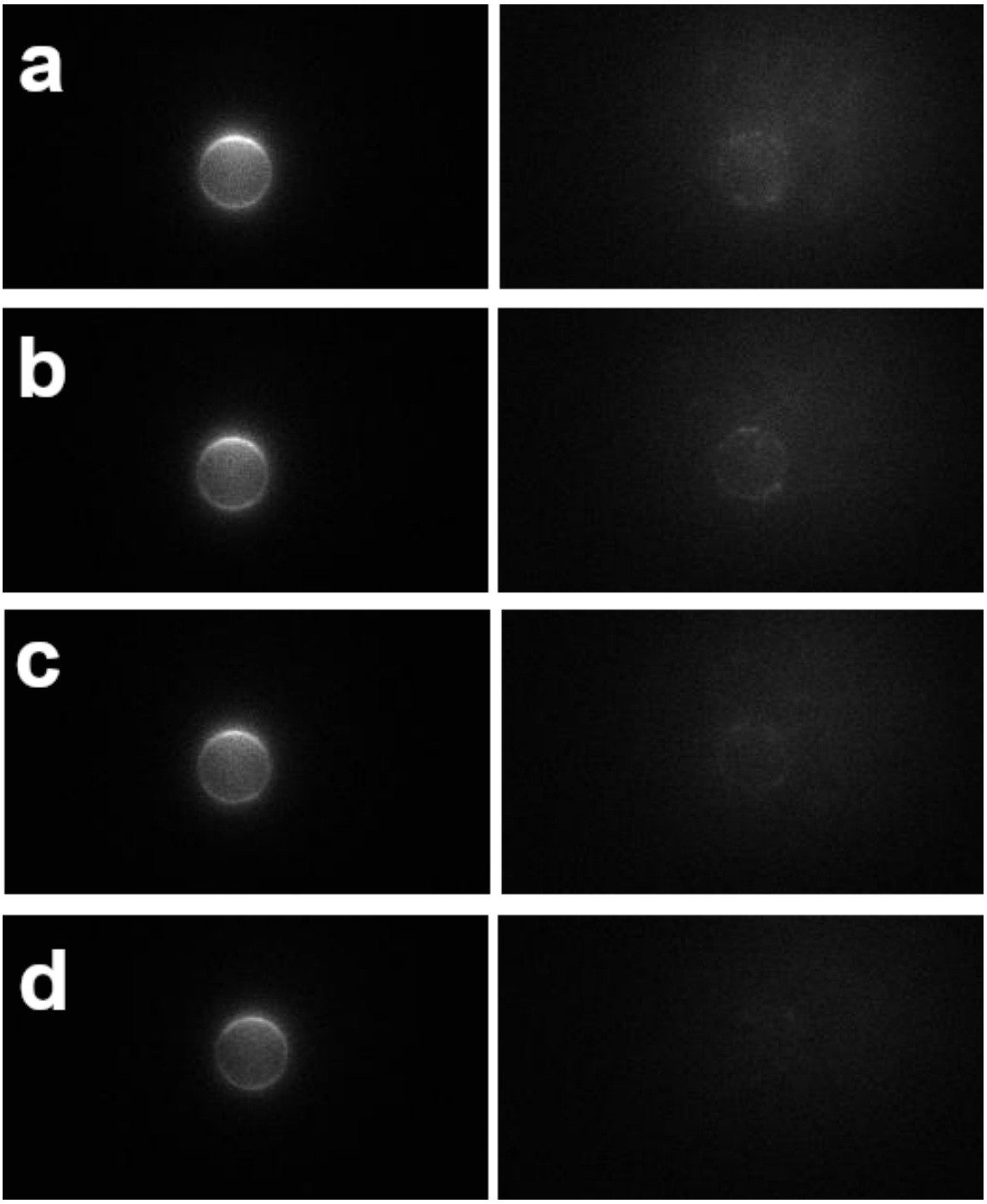

Figure 4.14: The left part of the images corresponds to the blue laser (wavelength 488 nm). The power of the blue laser is 1 mW. The right part of the images corresponds to the red laser (wavelength 640 nm). The power of the red laser is 6.4 mW. The exposure time for both images is 50 ms. **a:** snapshot of the video at 0 s. **b:** snapshot of the video at 1 s. **c:** snapshot of the video at 4 s. **d:** snapshot of the video at 35 s.

5 Conclusion

1. In this work it is shown that it is possible to dissolve L-α-PC LUVs into nanodiscs with the aid of Glyco-DIBMA. Different concentrations of Glyco-DIBMA in the LUV sample are tried out. The used mass fractions are $\frac{c_p}{c_l} = 0$, $\frac{c_p}{c_l} = 1.1$, $\frac{c_p}{c_l} = 2.2$ and $\frac{c_p}{c_l} = 11.2$. Nanodiscs formation is observed at $\frac{c_p}{c_l} = 1.1$. For higher concentrations of polymer a decrease in size is observable. All of the samples are checked in a FCS setup to verify the formation of nanodiscs.

2. Lipid only nanodiscs are mixed together with DPHPC SUVs to a lipid ratio of 1:10 of nanodiscs to SUVs. Gel assisted swelling is used to grow GUVS. Both SUVs are labeled with Atto 488 DPPE a blue lipid dye. GUVs are labeled with Atto 633 DPPE a red lipid dye. The sample is checked in a SMFM microscope and nanodiscs have formed GUVs togehter with SUVs.

3. Furthermore, it is possible to purify a membrane protein, namely GLIC, into nanodiscs with the aid of Glyco-DIBMA. The protein is purified via nickel affinity chromatography. The protein is on column labeled with Alexa 647 maleimide dye. Also here the sample is checked in a FCS setup to verify the formation of nanodiscs and the insertion of a protein into them.

4. Then these protein containing nanodiscs are also inserted into GUVs. The same aproach as for lipid only nanodiscs is used. The nanodisc to SUV lipid ratio is 1:20. The insertion of protein containing nanodiscs is observed and verified via a SMFM microscope.

Although these results look promising, further work needs to be done. A SDS-PAGE or Western-Blot of the protein nanodisc sample should be carried out, to verify if the protein of interest really inserted into nanodiscs. The low yield of GUVs and their small size is a problem. To tackle this issue Mg^{2+} could be used to get rid of Glyco-DIBMA. Furthermore

the buffer which contains the protein nanodiscs should be exchanged to a low salt buffer. This two approaches might lead to a suitable amount and size of the GUVs. Moreover, a method to check the labeling efficiency of the proteins should be developed to get a better estimate of the protein concentration and the lipid concentration in the sample. At last electrophysiology experiments with GUVs and inserted proteins should be carried out to verify if the protein is really functional. GUVs are useful biomimetic system as they are suited for microscopy and electrophysiology measurements. The reconstitution of membrane proteins into GUVs allows to investigate protein membrane interaction under controlled conditions. Like lipid composition, buffer composition inside and outside of the GUVs.

JOHANNES KEPLER
UNIVERSITY LINZ

Bibliography

[1] E. Wallin and G. von Heijne. “Genome-wide analysis of integral membrane proteins from eubacterial, archaean, and eukaryotic organisms”. In: *Protein science : a publication of the Protein Society* 7.4 (1998), pp. 1029–1038. DOI: 10.1002/pro.5560070420 (cit. on p. 7).

[2] Sinéad M. Smith. “Strategies for the Purification of Membrane Proteins”. In: *Methods in molecular biology (Clifton, N.J.)* 1485 (2017), pp. 389–400. DOI: 10.1007/978-1-4939-6412-3{\textunderscore}21 (cit. on p. 7).

[3] John P. Overington, Bissan Al-Lazikani, and Andrew L. Hopkins. “How many drug targets are there?” In: *Nature reviews. Drug discovery* 5.12 (2006), pp. 993–996. ISSN: 1474-1776. DOI: 10.1038/nrd2199 (cit. on p. 7).

[4] Natalie Bordag and Sandro Keller. “Alpha-helical transmembrane peptides: a "divide and conquer" approach to membrane proteins”. In: *Chemistry and physics of lipids* 163.1 (2010), pp. 1–26. DOI: 10.1016/j.chemphyslip.2009.07.009 (cit. on p. 7).

[5] Annela M. Seddon, Paul Curnow, and Paula J. Booth. “Membrane proteins, lipids and detergents: not just a soap opera”. In: *Biochimica et biophysica acta* 1666.1-2 (2004), pp. 105–117. ISSN: 0006-3002. DOI: 10.1016/j.bbamem.2004.04.011 (cit. on p. 7).

[6] Víctor Lórenz–Fonfría et al. “Solubilization, Purification, and Characterization of Integral Membrane Proteins”. In: *Production of membrane proteins*. Ed. by Anne Skaja Robinson. Vol. 244. Weinheim: Wiley-VCH, 2011, pp. 317–360. ISBN: 9783527327294. DOI: 10.1002/9783527634521.ch12 (cit. on p. 7).

[7] Zachary E. R. Newby et al. “A general protocol for the crystallization of membrane proteins for X-ray structural investigation”. In: *Nature protocols* 4.5 (2009), pp. 619–637. DOI: 10.1038/nprot.2009.27 (cit. on pp. 7, 8).

[8] Gilbert G. Privé. "Detergents for the stabilization and crystallization of membrane proteins". In: *Methods (San Diego, Calif.)* 41.4 (2007), pp. 388–397. ISSN: 1046-2023. DOI: 10.1016/j.ymeth.2007.01.007 (cit. on p. 8).

[9] Zhengrong Yang et al. "Membrane protein stability can be compromised by detergent interactions with the extramembranous soluble domains". In: *Protein science : a publication of the Protein Society* 23.6 (2014), pp. 769–789. DOI: 10.1002/pro.2460 (cit. on p. 8).

[10] Jean-Louis Rigaud, Bruno Pitard, and Daniel Levy. "Reconstitution of membrane proteins into liposomes: application to energy-transducing membrane proteins". In: *Biochimica et Biophysica Acta (BBA) - Bioenergetics* 1231.3 (1995), pp. 223–246. ISSN: 00052728. DOI: 10.1016/0005-2728(95)00091-V (cit. on p. 8).

[11] Ulrich H. N. Dürr, Ronald Soong, and Ayyalusamy Ramamoorthy. "When detergent meets bilayer: birth and coming of age of lipid bicelles". In: *Progress in nuclear magnetic resonance spectroscopy* 69 (2013), pp. 1–22. DOI: 10.1016/j.pnmrs.2013.01.001 (cit. on p. 8).

[12] Theresa M. Allen et al. "Detergent removal during membrane reconstitution". In: *Biochimica et Biophysica Acta (BBA) - Biomembranes* 601 (1980), pp. 328–342. ISSN: 00052736. DOI: 10.1016/0005-2736(80)90537-4 (cit. on p. 8).

[13] Ari Helenius and Kai Simons. "Solubilization of membranes by detergents". In: *Biochimica et Biophysica Acta (BBA) - Reviews on Biomembranes* 415.1 (1975), pp. 29–79. ISSN: 03044157. DOI: 10.1016/0304-4157(75)90016-7 (cit. on p. 8).

[14] Manuela Zoonens and Jean-Luc Popot. "Amphipols for each season". In: *The Journal of membrane biology* 247.9-10 (2014), pp. 759–796. DOI: 10.1007/s00232-014-9666-8 (cit. on p. 8).

[15] Jonas M. Dörr et al. "The styrene-maleic acid copolymer: a versatile tool in membrane research". In: *European biophysics journal : EBJ* 45.1 (2016), pp. 3–21. DOI: 10.1007/s00249-015-1093-y (cit. on pp. 8, 11, 13, 15).

[16] Ashley R. Long et al. "A detergent-free strategy for the reconstitution of active enzyme complexes from native biological membranes into nanoscale discs". In: *BMC biotechnology* 13 (2013), p. 41. DOI: 10.1186/1472-6750-13-41 (cit. on p. 9).

[17] I. G. Denisov et al. “Directed self-assembly of monodisperse phospholipid bilayer Nanodiscs with controlled size”. In: *Journal of the American Chemical Society* 126.11 (2004), pp. 3477–3487. ISSN: 0002-7863. DOI: 10.1021/ja0393574 (cit. on p. 9).

[18] Timothy H. Bayburt, Yelena V. Grinkova, and Stephen G. Sligar. “Self-Assembly of Discoidal Phospholipid Bilayer Nanoparticles with Membrane Scaffold Proteins”. In: *Nano Letters* 2.8 (2002), pp. 853–856. ISSN: 1530-6984. DOI: 10.1021/nl025623k (cit. on p. 9).

[19] Søren Roi Midtgaard et al. “Self-assembling peptides form nanodiscs that stabilize membrane proteins”. In: *Soft matter* 10.5 (2014), pp. 738–752. DOI: 10.1039/c3sm51727f (cit. on p. 9).

[20] Natanya R. Civjan et al. “Direct solubilization of heterologously expressed membrane proteins by incorporation into nanoscale lipid bilayers”. In: *BioTechniques* 35.3 (2003), pp. 556–60, 562–3. ISSN: 0736-6205. DOI: 10.2144/03353rr02 (cit. on p. 9).

[21] Huan-Xiang Zhou and Timothy A. Cross. “Influences of membrane mimetic environments on membrane protein structures”. In: *Annual review of biophysics* 42 (2013), pp. 361–392. DOI: 10.1146/annurev-biophys-083012-130326 (cit. on p. 10).

[22] Timothy J. Knowles et al. “Membrane proteins solubilized intact in lipid containing nanoparticles bounded by styrene maleic acid copolymer”. In: *Journal of the American Chemical Society* 131.22 (2009), pp. 7484–7485. ISSN: 0002-7863. DOI: 10.1021/ja810046q (cit. on p. 10).

[23] Abraham Olusegun Oluwole et al. “Solubilization of Membrane Proteins into Functional Lipid-Bilayer Nanodiscs Using a Diisobutylene/Maleic Acid Copolymer”. In: *Angewandte Chemie (International ed. in English)* 56.7 (2017), pp. 1919–1924. DOI: 10.1002/anie.201610778 (cit. on pp. 10, 14, 16, 35, 43).

[24] Abraham Olusegun Oluwole et al. “Formation of Lipid-Bilayer Nanodiscs by Diisobutylene/Maleic Acid (DIBMA) Copolymer”. In: *Langmuir : the ACS journal of surfaces and colloids* 33.50 (2017), pp. 14378–14388. DOI: 10.1021/acs.langmuir.7b03742 (cit. on pp. 10, 16, 35, 43).

[25] Bartholomäus Danielczak et al. “A bioinspired glycopolymer for capturing membrane proteins in native-like lipid-bilayer nanodiscs”. In: *Nanoscale* 14.5 (2022), pp. 1855–1867. DOI: 10.1039/D1NR03811G (cit. on pp. 10, 14, 16, 35, 43).

[26] Jonas M. Dörr et al. “Detergent-free isolation, characterization, and functional reconstitution of a tetrameric K+ channel: the power of native nanodiscs”. In: *Proceedings of the National Academy of Sciences of the United States of America* 111.52 (2014), pp. 18607–18612. DOI: 10.1073/pnas.1416205112 (cit. on pp. 10, 13).

[27] David J. K. Swainsbury et al. “The effectiveness of styrene-maleic acid (SMA) copolymers for solubilisation of integral membrane proteins from SMA-accessible and SMA-resistant membranes”. In: *Biochimica et Biophysica Acta (BBA) - Biomembranes* 1859.10 (2017), pp. 2133–2143. ISSN: 00052736. DOI: 10.1016/j.bbamem.2017.07.011 (cit. on p. 13).

[28] Debajyoti Dutta et al. “Expression and detergent free purification and reconstitution of the plant plasma membrane Na+/H+ antiporter SOS1 overexpressed in Pichia pastoris”. In: *Biochimica et biophysica acta. Biomembranes* 1862.3 (2020), p. 183111. DOI: 10.1016/J.BBAMEM.2019.183111 (cit. on p. 13).

[29] Kerrie A. Morrison et al. “Membrane protein extraction and purification using styrene-maleic acid (SMA) copolymer: effect of variations in polymer structure”. In: *The Biochemical journal* 473.23 (2016), pp. 4349–4360. DOI: 10.1042/BCJ20160723 (cit. on p. 13).

[30] Anne Grethen et al. “Thermodynamics of nanodisc formation mediated by styrene/maleic acid (2:1) copolymer”. In: *Scientific reports* 7.1 (2017), p. 11517. DOI: 10.1038/s41598-017-11616-z (cit. on p. 13).

[31] Rosa Catania et al. “Detergent-Free Functionalization of Hybrid Vesicles with Membrane Proteins Using SMALPs”. In: *Macromolecules* 55.9 (2022), pp. 3415–3422. ISSN: 0024-9297. DOI: 10.1021/acs.macromol.2c00326 (cit. on pp. 13, 40).

[32] Benjamin D. Harding et al. “Characterizing the structure of styrene-maleic acid copolymer-lipid nanoparticles (SMALPs) using RAFT polymerization for membrane protein spectroscopic studies”. In: *Chemistry and physics of lipids* 218 (2019), pp. 65–72. DOI: 10.1016/j.chemphyslip.2018.12.002. (cit. on p. 16).

[33] Wikipedia. *Stokes' law*. URL: https://upload.wikimedia.org/wikipedia/commons/thumb/a/ae/Stokes_sphere.svg/800px-Stokes_sphere.svg.png (visited on 05/24/2022) (cit. on p. 17).

[34] Keith J. Laidler and John H. Meiser. *Physical chemistry*. Menlo Park/Calif.: Benjamin/Cummings, 1982. ISBN: 0805356827 (cit. on p. 16).

[35] Robert Byron Bird, Warren E. Stewart, and Edwin N. Lightfoot. *Transport phenomena*. 2. ed., Wiley internat. ed. New York and Weinheim: Wiley, 2002. ISBN: 0471410772. URL: http://www.loc.gov/catdir/description/wiley036/2001023739.html (cit. on p. 16).

[36] Tuhin Samanta and Dmitry V. Matyushov. "Mobility of large ions in water". In: *The Journal of Chemical Physics* 153.4 (2020), p. 044503. ISSN: 0021-9606. DOI: 10.1063/5.0014188. URL: https://aip.scitation.org/doi/10.1063/5.0014188 (cit. on p. 16).

[37] John Happel and Howard Brenner. "The Motion of a Rigid Particle of Arbitrary Shape in an Unbounded Fluid". In: *Low Reynolds number hydrodynamics*. Ed. by R. J. Moreau, John Happel, and Howard Brenner. Vol. 1. Mechanics of fluids and transport processes. Dordrecht: Springer Netherlands, 1981, pp. 159–234. ISBN: 978-90-247-2877-0. DOI: 10.1007/978-94-009-8352-6{\textunderscore}5 (cit. on p. 17).

[38] Barbara A. Lewis and Donald M. Engelman. "Lipid bilayer thickness varies linearly with acyl chain length in fluid phosphatidylcholine vesicles". In: *Journal of Molecular Biology* 166.2 (1983), pp. 211–217. ISSN: 00222836. DOI: 10.1016/s0022-2836(83)80007-2 (cit. on p. 17).

[39] Pouyan Khakbaz and Jeffery B. Klauda. "Probing the importance of lipid diversity in cell membranes via molecular simulation". In: *Chemistry and physics of lipids* 192 (2015), pp. 12–22. DOI: 10.1016/j.chemphyslip.2015.08.003 (cit. on p. 17).

[40] Zaigao Tan et al. "Engineering Escherichia coli membrane phospholipid head distribution improves tolerance and production of biorenewables". In: *Metabolic engineering* 44 (2017), pp. 1–12. DOI: 10.1016/j.ymben.2017.08.006 (cit. on p. 17).

[41] Himanshu Pandey, Radha Rani, and Vishnu Agarwal. "Liposome and Their Applications in Cancer Therapy". In: *Brazilian Archives of Biology and Technology* 59.0 (2016). DOI: 10.1590/1678-4324-2016150477 (cit. on p. 19).

[42] Matthias Garten et al. "Reconstitution of a transmembrane protein, the voltage-gated ion channel, KvAP, into giant unilamellar vesicles for microscopy and patch clamp studies". In: *Journal of visualized experiments : JoVE* 95 (2015), p. 52281. DOI: 10.3791/52281 (cit. on pp. 20, 21, 36, 46).

[43] Avanti Polar Lipids. *DPHPC*. 2022. URL: https://avantilipids.com/product/850356 (visited on 05/24/2022) (cit. on p. 20).

[44] Victor Martin Bolanos-Garcia and Owen Richard Davies. "Structural analysis and classification of native proteins from E. coli commonly co-purified by immobilised metal affinity chromatography". In: *Biochimica et biophysica acta* 1760.9 (2006), pp. 1304–1313. ISSN: 0006-3002. DOI: 10.1016/j.bbagen.2006.03.027 (cit. on p. 22).

[45] R. Czoik et al. "Complexes of Silver with Histidine and Imidazole Investigated by the Calorimetric and Potentiometric Methods". In: *Acta Physica Polonica A* 114.6A (2008), A-51-A–56. ISSN: 0587-4246. DOI: 10.12693/APhysPolA.114.A-51 (cit. on p. 23).

[46] Wikipedia. *L-Cysteine*. URL: https://en.wikipedia.org/wiki/Cysteine#/media/File:L-Cystein_-_L-Cysteine.svg (visited on 06/06/2022) (cit. on p. 23).

[47] AAT Bioquest, Inc., ed. 2021. URL: https://images.aatbio.com/products/figures-and-data/ifluor-430-maleimide/figure-for-ifluor-430-maleimide_KaEsK.jpg (visited on 05/24/2022) (cit. on p. 24).

[48] Michael J. Sanderson et al. "Fluorescence microscopy". In: *Cold Spring Harbor protocols* 2014.10 (2014), pdb.top071795. DOI: 10.1101/pdb.top071795 (cit. on p. 25).

[49] Kaloian Koynov and Hans-Jürgen Butt. "Fluorescence correlation spectroscopy in colloid and interface science". In: *Current Opinion in Colloid & Interface Science* 17.6 (2012), pp. 377–387. ISSN: 13590294. DOI: 10.1016/j.cocis.2012.09.003 (cit. on pp. 25, 26).

[50] E. P. Petrov and P. Schwille. "State of the Art and Novel Trends in Fluorescence Correlation Spectroscopy". In: *Standardization and Quality Assurance in Fluorescence Measurements II*. Ed. by Ute Resch-Genger. Vol. 6. Springer Series on Fluorescence. Berlin, Heidelberg: Springer Berlin Heidelberg, 2008, pp. 145–197. ISBN: 978-3-540-70570-3. DOI: 10.1007/4243{\textunderscore}2008{\textunderscore}032 (cit. on pp. 27, 28, 29).

[51] Radek Macháň and Thorsten Wohland. "Recent applications of fluorescence correlation spectroscopy in live systems". In: *FEBS letters* 588.19 (2014), pp. 3571–3584. DOI: 10.1016/j.febslet.2014.03.056 (cit. on p. 28).

[52] Rodrigo Cuevas Arenas et al. "Influence of lipid bilayer properties on nanodisc formation mediated by styrene/maleic acid copolymers". In: *Nanoscale* 8.32 (2016), pp. 15016–15026. DOI: 10.1039/c6nr02089e (cit. on pp. 35, 43).

[53] L. D. Mayer, M. J. Hope, and P. R. Cullis. "Vesicles of variable sizes produced by a rapid extrusion procedure". In: *Biochimica et Biophysica Acta (BBA) - Biomembranes* 858.1 (1986), pp. 161–168. ISSN: 00052736. DOI: 10.1016/0005-2736(86)90302-0 (cit. on p. 35).

[54] M. J. Hope et al. "Production of large unilamellar vesicles by a rapid extrusion procedure. Characterization of size distribution, trapped volume and ability to maintain a membrane potential". In: *Biochimica et Biophysica Acta (BBA) - Biomembranes* 812.1 (1985), pp. 55–65. ISSN: 00052736. DOI: 10.1016/0005-2736(85)90521-8 (cit. on p. 35).

[55] Z. Fourati and M. Delarue. *Xray structure of GLIC in complex with crotonate*. 2019. DOI: 10.2210/pdb6hji/pdb (cit. on p. 43).

[56] W. Dowhan. "Molecular basis for membrane phospholipid diversity: why are there so many lipids?" In: *Annual review of biochemistry* 66 (1997), pp. 199–232. ISSN: 0066-4154. DOI: 10.1146/annurev.biochem.66.1.199 (cit. on p. 44).

[57] A. M. Bouchet et al. "Structural and dynamical surface properties of phosphatidylethanolamine containing membranes". In: *Biochimica et biophysica acta* 1788.5 (2009), pp. 918–925. ISSN: 0006-3002. DOI: 10.1016/j.bbamem.2009.02.012 (cit. on p. 44).

[58] Avanti Polar Lipids. *DOPE*. 2022. URL: https://avantilipids.com/product/850725 (visited on 05/24/2022) (cit. on p. 44).